

What is resolution? A statistical minimax testing perspective on super-resolution microscopy

GYTIS KULAITIS

`gytis.kulaitis@mathematik.uni-goettingen.de`
Institute for Mathematical Stochastics, University of Göttingen

AXEL MUNK

`munk@math.uni-goettingen.de`
Institute for Mathematical Stochastics, University of Göttingen
and
Felix Bernstein Institute for Mathematical Statistics in the Bioscience,
University of Göttingen
and
Max Planck Institute for Biophysical Chemistry, Göttingen, Germany

FRANK WERNER¹

`frank.werner@mathematik.uni-wuerzburg.de`
Institute of Mathematics, University of Würzburg

As a general rule of thumb the resolution of a light microscope (i.e. the ability to discern objects) is predominantly described by the full width at half maximum (FWHM) of its point spread function (psf)—the diameter of the blurring density at half of its maximum. Classical wave optics suggests a linear relationship between FWHM and resolution also manifested in the well known Abbe and Rayleigh criteria, dating back to the end of 19th century. However, during the last two decades conventional light microscopy has undergone a shift from microscopic scales to nanoscales. This increase in resolution comes with the need to incorporate the random nature of observations (light photons) and challenges the classical view of discernability, as we argue in this paper. Instead, we suggest a statistical description of resolution obtained from such random data. Our notion of discernability is based on statistical testing whether one or two objects with the same total intensity are present. For Poisson measurements we get linear dependence of the (minimax) detection boundary on the FWHM, whereas for a homogeneous Gaussian model the dependence of resolution is nonlinear. Hence, at small physical scales modeling by homogeneous gaussians is inadequate, although often implicitly assumed in many reconstruction algorithms. In contrast, the Poisson model and its variance stabilized Gaussian approximation seem to provide a statistically sound description of resolution at the nanoscale. Our theory is also applicable to other imaging setups, such as telescopes.

Keywords: Microscopy, (super)resolution, nanoscopy, minimax, detection boundary, equivalence of experiments.

AMS classification numbers: 60F05, 62B10, 62C20, 91B06, 94A12, 94A13, 94A15, 94A17.

¹Corresponding author

1 Introduction

1.1 Lens optics and diffraction

According to geometrical optics, an ideal light microscope would be able to distinguish two points in space being arbitrary close. However, in 1873 Abbe [1] formulated what later became known as the *Abbe diffraction limit* (Figure 1C): Two points can be resolved only if their distance d in space is at least

$$d = \frac{\lambda}{2\text{NA}}, \quad (1)$$

where λ is the wavelength of incoming light and NA is the numerical aperture of the microscope. The numerical aperture is equal to the product of the refractive index of the medium (1 for vacuum, ≈ 1 for air) and the sine of one-half of the angle of the cone of light that can enter the microscope. Abbe [1] argued that diffraction and interference of light have to be taken into account when distances in the order of the wavelength of the illumination light are considered (see [14] and references therein for a comprehensive account). This paradigm has limited light microscopy for more than a century until the ground-breaking advent of super-resolution microscopy [29], see Section 1.2. For the following, it is beneficial to recall the basic physics tailored to our needs, see also [5].

Given a specimen under the microscope f , due to diffraction (and the resulting interference, see Figure 1A and B) the imaging system causes a blur so that we do not simply observe an M times magnified image of f . This blur is usually obtained by calculating analytically or estimating from data the blur pattern of a single point—the point spread function (psf) h . For an incoherent imaging system, e.g. a fluorescence microscope, using Huygens’s principle, the image of the specimen then can be obtained by summing up the blurred images of the points constituting the sample. This results in a convolution

$$g(x) = \int_O h(x - Mx') f(x') dx', \quad (2)$$

where O is the space containing the specimen—the object space—and $f : O \rightarrow \mathbb{R}$. The space consisting of magnified points Mx' is called the image space I and $g : I \rightarrow \mathbb{R}$ is the image of the specimen.

If the microscope was perfect and there was no blur, then the psf h would simply correspond to a delta function $\delta_{x-Mx'}$, so that $g(x) = f(x/M)$. In general, the psf h can be computed explicitly by scalar diffraction theory. Under the assumption of circular aperture and using the paraxial approximation [10, 49], h becomes proportional to the Airy pattern [3] (Figure 1A)

$$h(x) \propto \left| 2A \left(\frac{2\pi \text{NA}}{\lambda M} \|x\|_2 \right) \right|^2, \quad (3)$$

where λ is the illumination wavelength and $\|\cdot\|_2$ is the Euclidean norm. The function A in (3) is given by $A(u) = J_1(u)/u$, where J_1 is the Bessel function of the first kind.

Independently of Abbe, Lord Rayleigh formulated in 1879 a resolution criterion for spectroscopes [60]. Applied to microscopes Rayleigh’s criterion reads that two point sources at x_1 and x_2 having equal intensity can just be resolved if the central maximum of the first psf centered at x_1 coincides with the first minimum of the second psf. The first zero of the Bessel function J_1 is at $x \approx 3.8317$ and hence $x/2\pi \approx 0.6098$. Thus, in the case of circular aperture the Rayleigh criterion is given by

$$d = 0.61 \frac{\lambda}{\text{NA}}. \quad (4)$$

Note that this is slightly more conservative than Abbe’s result (1). See Figure 1C and D for a comparison.

The resolution criteria (1) and (4) can be understood in terms of the full width at half maximum (FWHM) of the (effective) psf (see Figure 1B, where $\text{FWHM} = |x_2 - x_1|$). More precisely, the

FWHM is defined as the width of the psf when its intensity is half of its maximal intensity. The ability to state both Abbe and Rayleigh criteria in terms of the FWHM has led to the common understanding that two point sources in space can be resolved by a light microscope as soon as their distance is larger than roughly the FWHM of the psf h . Usage of the FWHM as a resolution criterion dates back to at least 1927 [35] and is still popular today [19]. The FWHM criterion is particularly well-suited if the psf can be approximated by a Gaussian kernel as shown in Figure 1B, since this function does not have any local minima. In fact, the approximation of the psf by a Gaussian is very common and sufficient for many practical purposes, see e.g. [67]. For an Airy pattern (3), the FWHM can be computed by first computing the FWHM of $A(u)^2 = (J_1(u)/u)^2$, which—due to $\max_u A(u)^2 = A(0)^2 = 1$ —is determined by the solution of $J_1(u) = \pm u/\sqrt{2}$. This yields an FWHM of 3.232 for $A(u)^2$, and hence taking the additional scaling factors in (3) into account together with $Mx' = x$, we get the FWHM resolution criterion in its most common form

$$d = \text{FWHM} = 0.51 \frac{\lambda}{\text{NA}}. \quad (5)$$

Thus, the FWHM limit is almost equal to the Abbe resolution limit (1) and somewhat below the Rayleigh resolution limit (4).

We mention that due to their generality, the above resolution criteria are not confined to microscopes and can also be applied to telescopes [2, 7], or other imaging devices, in general. We stress that there are many other resolution criteria such as the recently popularized Fourier ring correlation [6], which can be expressed in terms of the FWHM as well.

Concerning microscopes, from Equations (1), (4) and (5) it seems that there are only two possible ways to improve the resolution: either the wavelength has to be decreased, or the numerical aperture increased. Since the wavelength λ is inversely proportional to the energy of the incoming light, decreasing the wavelength might damage the sample, a major issue in living cell microscopy. Hence, visible light (380–760 nm) is preferred for such applications. Concerning the second option, the numerical aperture of a modern lens is around 1.3–1.5 [67], and this value has not improved substantially during the last decades. In fact, Abbe’s resolution limit has been standing as a paradigm for more than hundred years [29], limiting conventional light microscopes to about 250 nm lateral and 500 nm axial resolution¹ [8, 28, 14, 27].

1.2 From microscopy to nanoscopy

One important idea to improve on Abbe’s resolution limit is confocal microscopy suggested by Minsky [45, 51] in 1961. Here only a small spot of the object is illuminated at any given time, and non-focused light is blocked by a pinhole. Moving the pinhole over the sample (scanning) creates multiple images which are then combined to produce the full image. Clearly, the smaller the pinhole, the more the resolution is increased. On the other hand, a smaller pinhole decreases the overall image intensity. Theoretically confocal microscopy increases the resolution by $\sqrt{2}$, see e.g. [19] or [28], but due to these competing effects practical increase is lower. Consequently, although providing some improvement, confocal microscopy on its own cannot break the resolution barrier [5].

An early approach to overcome Abbe’s resolution limit relies on the fact that both limits in Equations (1) and (4) are only valid in the *far-field*, i.e. when sample and microscope are sufficiently far apart. Similarly, the regime when the sample and the microscope are less than a wavelength apart is called *near-field*. In this case, the size of the aperture and not the wavelength determines the resolution [13]. In 1972 Ash and Nicholls [4] went below Abbe’s diffraction limit in the near-field. Using 3 cm wavelength they achieved a resolution of $\lambda/60$. Current experiments are able to achieve a lateral resolution of 20 nm and a vertical resolution of 2–5 nm [18, 50]. Although impressive, near-field microscopes have certain disadvantages, the most obvious being that the

¹ Axial resolution is the resolution in the longitudinal direction of the measurement trajectory (z -axis), whereas lateral resolution is the resolution in the image plane (x, y). Note that the Abbe and Rayleigh criteria in (1) and (4) hold for lateral resolution.

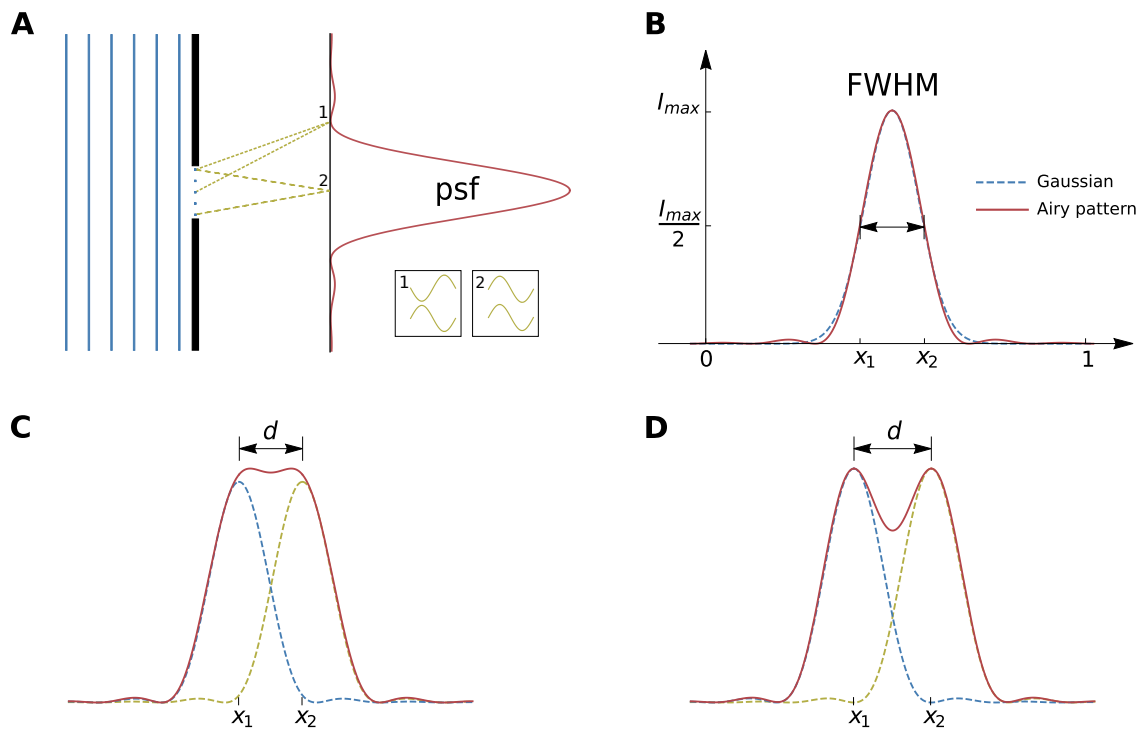


Figure 1: (A) 1D view of a 2D wave traveling through a circular aperture of width on the same order as the wavelength. By Huygen's principle each point on a wavefront acts as a point source (5 points shown). Due to diffraction and interference an Airy pattern is formed—where the light interferes constructively/destructively we get (local) maxima/minima in the intensity pattern. If the distance between the aperture and the screen is much larger than the wavelength, the slit acts as a point light source. (B) Approximation of an Airy pattern centered at $\frac{1}{2}(x_1 + x_2)$ by a Gaussian profile matching the maxima with the FWHM indicated. (C)/(D) Two Airy patterns centered at x_1 and x_2 , distance $(1)/(4)$ apart, and their superposition (solid red).

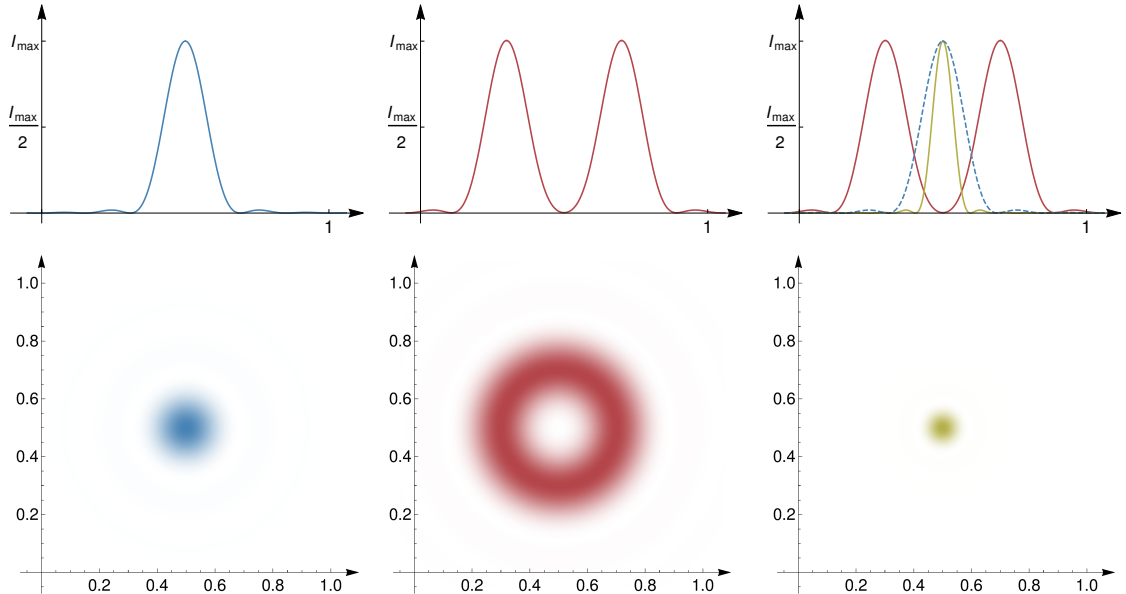


Figure 2: STED microscopy. Column I: Original psf (blue), Column II: Depletion psf (red), Column III: effective psf (solid beige). The top row shows psfs in 1D, the bottom row in 2D.

specimen must be very close to the microscope and one is hence mostly limited to surface measurements. Moreover, they are unsuitable for transparent objects which excludes many biological samples.

The major breakthrough to overcome Abbe’s diffraction limit using far-field microscopy dates back to a fundamental paper by S. W. Hell and J. Wichman [29] and is intimately related to the development of photoswitchable fluorophores [28, 36] which can be switched on and off in a statistically controlled manner. After a laser excitation they emit light of higher wavelength (less energy) than absorbed due to rotational and vibrational losses. Exploiting this, the sample is—just as in confocal microscopy—scanned along a grid by illuminating it with a (pulsed) excitation beam focused at the current grid point and only the resulting fluorescence is measured. Using a dichroic beamsplitter, it is ensured that only the fluoresced light is detected at the detector. On each grid point this procedure is repeated for a fixed time (the pixel dwell time) t or equivalently for a fixed number of pulses (also denoted by t). Therefore, one is able to image specific predefined structures, instead of observing a superposition of the whole sample. The fundamental importance of this principle and its impact on modern life sciences, among others, is reflected in the 2014 Nobel prize in Chemistry “for the development of super-resolved fluorescence microscopy” [21], where the term *super-resolution* refers to any technique, which is able to break Abbe’s diffraction limit in the far field. Nowadays there exist two main approaches to photoswitching:

Scanning mode: In the scanning mode, non-linearity of the response to excitation is exploited and dyes in a pre-defined region are shut off to enhance resolution. We do not aim to describe all possible approaches here in detail (see, e.g., [69] or [5] for a survey accessible to a statistical audience) and confine our representation to the most prominent state-of-the-art scanning mode super-resolution technique—Stimulated Emission Depletion (STED) [29, 28, 37, 19]. In STED the fluorescent dyes are only excited in the center of a torus shaped region and are actively depleted inside the torus, see Figure 2.

To analyze the resolution of a STED super-resolution microscope, we can still employ an analog to Rayleigh’s criterion (4) by computing the effective psf, see Figure 2. This leads to a resolution criterion of the form

$$d = \frac{\lambda}{2NA\sqrt{1+\xi}}, \quad (6)$$

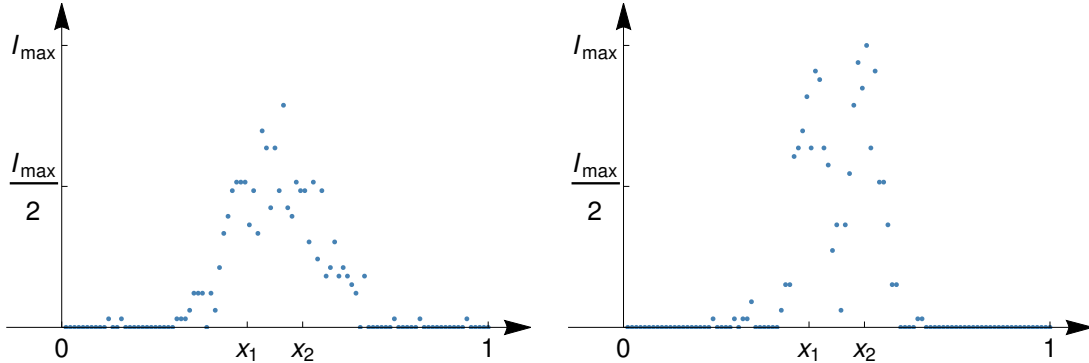


Figure 3: Photons generated by two point sources at x_1 and x_2 which are hard to distinguish for a conventional light microscope having Airy psf (3), but are easily distinguishable with narrower effective psf after STED.

see [28, 68], where $\xi > 0$ is the shrinkage factor increasing in the direction of maximal intensity within the depletion spot. Note that, in principle, the resolution can be increased arbitrarily by increasing ξ . However, in practice, this leads to a decreased number of measured photons in view of the thinner psf and hence to a decreased signal-to-noise ratio. We will discuss this trade-off in Section 1.7. In experiments, resolutions of around 2.4 nm have been achieved this way, see [54].

Stochastic mode: In the stochastic mode, chemical complexity of dyes is exploited, forcing them to emit light at separate times which makes them resolvable in time. As an example, we mention Single Marker Switching (SMS) nanoscopy in its various variants [8, 55, 33, 26, 20], see also [59] for a survey from a statistical perspective and [17] for a survey on single-molecule techniques. Here one excites only a few dyes per pulse by using only a small illumination intensity. Hence, only single dyes which are spatially well separated are excited in each pulse with high probability. Consequently, there is no need to distinguish between two or more point sources, and thus from this point of view the resolution is arbitrarily small. However, the actual limitation is given by the localization accuracy when estimating the position of each fluorophore by the center of the observed psf (without any need for deconvolution). This can be understood from a statistical point of view as estimating the mean μ of a distribution by its empirical mean. Let N be the random number of photons observed in a small region of space and denote by X_1, \dots, X_N their spatial positions. Note that N depends on the illumination time $t > 0$, which can be chosen in the experimental setup, and $\mathbb{E}[N] \sim t$ (in our model to be introduced below, we in fact have $\mathbb{E}[N] = t$, see Section 1.3). Then in two dimensions the CLT yields

$$\sqrt{N} \left(\frac{1}{N} \sum_{i=1}^N X_i - \mu \right) \rightarrow^{\mathcal{D}} \mathcal{N}_2(0, \Sigma) \quad \text{as } t \rightarrow \infty, \quad \text{a.s.}$$

with a covariance matrix Σ given in terms of the psf h . Thus, neglecting the background and pixelation noise, the position of the sample's center can be estimated as the average of the fluorophore centers leading to the localization error

$$d \sim \frac{1}{\sqrt{\mathbb{E}[N]}}, \quad (7)$$

see [64]. This can be made more precise in terms of confidence circles for the true position of the dye as shown in Figure 4. Note that although (7) suggests that the resolution can be increased indefinitely, in practice the number of observable photons is limited due to the dyes suffering from photodamage which causes them to bleach and hence to lose the ability to fluoresce.

Comparing (6) and (7) reveals a gap in the common understanding of *resolution* (as in (1), (4) and (6)) and *localization accuracy* (as in (7)), namely that both the experimental setup **and**

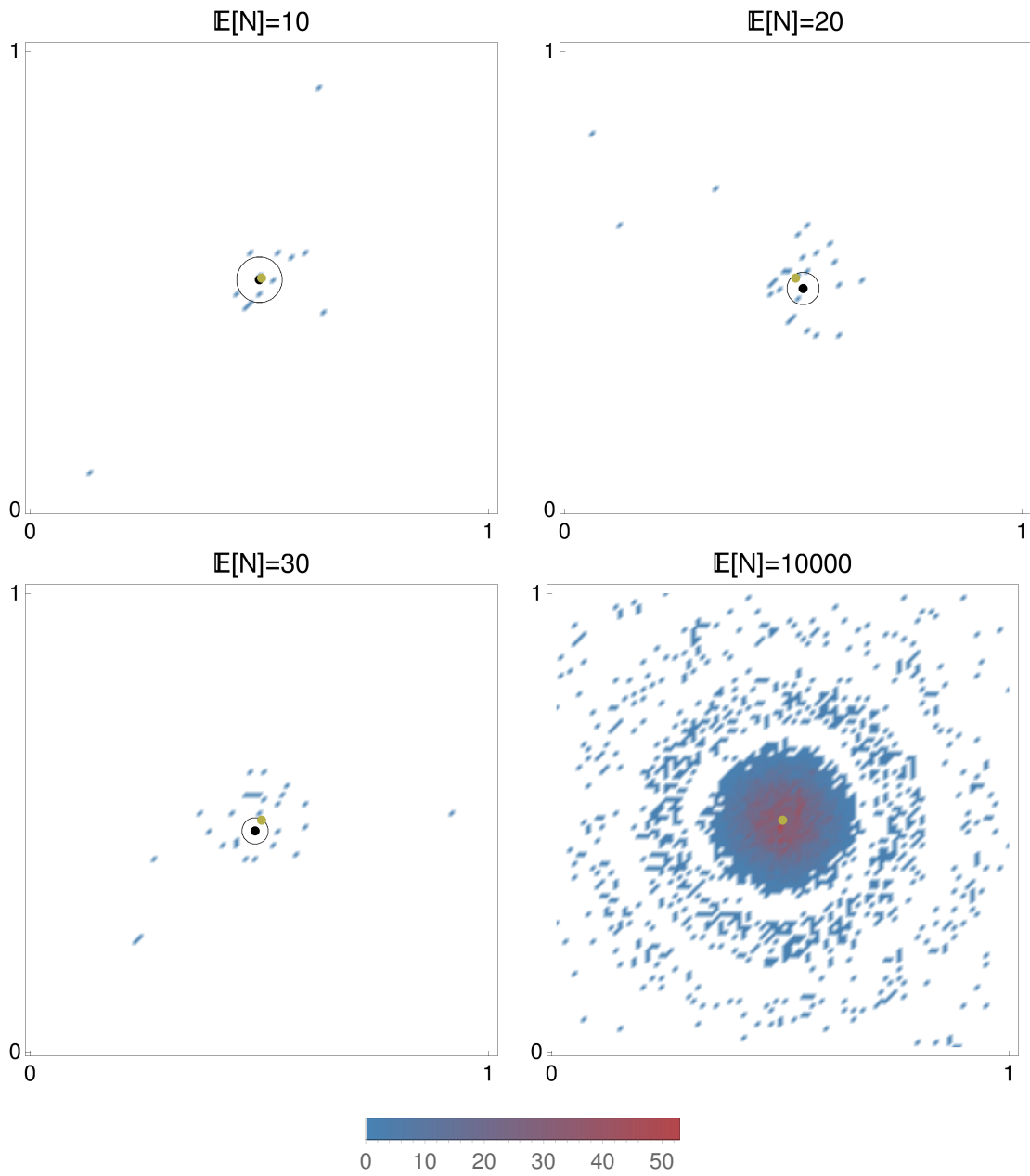


Figure 4: Illustration of localization error in SMS microscopy (7). The psf h was chosen to be the Airy pattern. The beige dots mark the center of the Airy distribution $(0.5, 0.5)$ and the black dots the empirical means. The black circles correspond to the 90% confidence circles under the described CLT.

the statistical error should play a role in the actual resolution of a (super-resolution) microscope. In fact, in any real world experiment, the noise plays a central role for the actual ability to distinguish two point sources, leading to the conclusion that the noise level (e.g. the observed number of photons) should also play a role in Equations (1), (4) and (6). This plays a minor role on the microscopic scale but becomes more severe as resolution increases, especially at the nanoscale. In addition, the effective psf should also affect the localization accuracy in (7). Given the vast applications of microscopy and rapid progress of super-resolution, a refined understanding of fundamental principles governing resolution is of immense importance. However, as far as we know, such mathematically rigorous model of statistical resolution is still lacking. To overcome this gap, in this paper we aim to provide unifying modeling (see Section 1.3) and statistical analysis (Sections 1.4 to 1.7), which allow to understand both the effect of the experimental setup (in terms of the convolution in (2)) and the random nature of photon counts on the resulting resolution.

1.3 Statistical model

To derive a mathematically rigorous formulation for the resolution of a (fluorescence) microscope with psf h , we start with modeling the actual observations. Throughout this paper we confine ourselves to the one-dimensional problem which is a prototype for higher spatial dimensions (see Remark 1.2 below).

In practice, the physical space O is scanned bin-wise or sampled at once by a CCD camera or another detection device. We will assume that the image space I , the space of magnified points, is the unit interval $[0, 1]$, and each scanned bin in O corresponds to a bin $B_i = [(i-1)/n, i/n] \subset I$. From a mathematical point of view, we can for most experimental setups also re-scale $O = [0, 1]$, and in this case scanning at a bin B_i means to center the psf at the center of B_i . Each bin is either illuminated $t \in \mathbb{N}$ times by a short excitation pulse (pulsed illumination), or it is illuminated continuously for some time t (continuous illumination) which we may also assume to be an integer due to time discretization in the measurement process (e.g. t can denote time in pico- or nanoseconds). For each bin we observe the total number of detected photons denoted by $Y_i \in \mathbb{N}$. Clearly, Y_i is a random quantity, but according to the above reasoning, we may assume that

$$\mathbb{E}[Y_i] = t \int_{B_i} g(x) dx, \quad (8)$$

where g is the image of the specimen as defined in (2). We assume here and in the following that the statistical experiments when measuring at B_i are independent for different values of i , which is physically evident in many measurement settings, see e.g. [5, 34]. Consequently, we observe a vector $(Y_i)_{i \in \{1, \dots, n\}}$ of independent random variables

$$Y_i \stackrel{\text{indep.}}{\sim} F_{t \int_{B_i} g(x) dx}, \quad i \in \{1, \dots, n\} \quad (9)$$

with a family of distributions $F_{t\theta}$ for parameters $\theta \in (0, \infty)$ in mean value parametrization.

The specific choice of $F_{t\theta}$ depends fundamentally on the imaging setup and on the number of photons collected. We consider the following scenarios here:

Poisson model (P) The finest model we will consider here is a Poisson model $F_{t\theta} = \text{Poi}(t\theta)$. This is well-known and widely used in the literature, see e.g. [7, 34]. It is often derived in the setting of continuous illumination, but the Poisson model can also be motivated by means of the law of small numbers, see e.g. [47].

Variance stabilized Gaussian model (VSG) Due to the central limit theorem, for sufficiently large t also normal models appear a reasonable approximation. Following the previous reasoning, this then leads to $\mathcal{N}(t\theta, t\theta)$. Applying the variance stabilizing transform $f(x) = 2\sqrt{x}$, we thus analyze $F_{2\sqrt{t\theta}} = \mathcal{N}(2\sqrt{t\theta}, 1)$.

Homogeneous Gaussian model (HG) The simplest model to assume in this situation is the homogeneous Gaussian model $\mathcal{N}(\mu, \sigma^2)$ for some general mean $\mu = t\theta$ and some constant

variance σ^2 . In particular, many recovery algorithms rely on this model assumption, see e.g. [7, 34] for further discussion. After re-normalizing the mean μ by σ , we can w.l.o.g. set $\sigma = 1$ and consider the model $\mathcal{N}(t\theta, 1)$.

For a comprehensive discussion and more details on the modeling see e.g. [5, 47]. We emphasize that the homogeneous Gaussian model is commonly used as a proxy for “microscopy with noise” and has been investigated in many studies. We will, however, show that it is misleading in the present context. In contrast, we will show that the other two models (asymptotically) lead to the same resolution which scales linearly with the FWHM in agreement with the physical understanding.

Remark 1.1. We consider photons, but treat them as classical particles. In the case of Poisson model, our modeling as given in (8) and (9) corresponds to the so-called *semiclassical detection model*, see e.g. Chapter 9 of [23]. This model is an approximation and follows from the general theory of light and matter interactions—quantum electrodynamics (QED), see e.g. [41] and in particular its Appendix B.

1.4 Statistical testing problem

Building on the models in Section 1.3, in the following we will describe the resolution of a microscope with psf $h \geq 0$ as a detection problem. We consider general psfs and provide a mathematically rigorous (asymptotic) statistical testing theory for resolution. To this end, we test the hypothesis that there is one point source at x'_0 against the alternative that there are two equally bright point sources at x'_1 and x'_2 , respectively. This reflects the ability to discern between one and two objects, and is in line with many common resolution criteria, see e.g. [15]. Taking into account the previous considerations on diffraction, in particular (2), and setting $x_i = Mx'_i$ for $i \in \{0, 1, 2\}$ we hence consider testing the hypothesis that

$$H_0 : g(x) = h(x - x_0) \tag{10a}$$

against the alternative

$$H_1 : g(x) = \frac{1}{2} h(x - x_1) + \frac{1}{2} h(x - x_2), \tag{10b}$$

see Figure 5 for an illustration. The factors of 1/2 in the alternative ensure that the image g has the same intensity under H_0 and H_1 (for generalizations to $qh(x - x_1) + (1 - q)h(x - x_2)$ with $q \in (0, 1)$ see Section 3.4). We always assume that x_0 is fixed. For each particular alternative, we also assume that x_1 and x_2 are fixed as well. However, in the asymptotic analysis we will let $d = |x_1 - x_2| \rightarrow 0^2$ and later on we will consider the worst case scenario (Theorem 1.3). Without loss of generality, we scale the image function g in (10) to be defined on the unit interval $[0, 1]$ and normalize it to have volume 1. Setting the domain of g to be the unit interval $[0, 1]$ allows us to interpret $h(\cdot - x_i)$ as functions with domain $[0, 1]$ for $i \in \{0, 1, 2\}$.

Remark 1.2. Note that in practice, the hypothesis testing problem (10) occurs in multiple dimensions (depending on the observational setup). However, if $x_0, x_1, x_2 \in [0, 1]^m$, $m \geq 1$, the statistically most difficult situation, independently of the (spatial) dimension m , is if all three points fall on a line, as otherwise the distributions under H_0 and H_1 would not have the same center of mass. Therefore, the whole problem can essentially be reduced to the one-dimensional problem of testing on this line.

A (*randomized*) statistical test for the hypothesis testing problem (10) is a measurable map $\Phi_n : \mathbb{R}^n \rightarrow [0, 1]$, $n \in \mathbb{N}$, where $\Phi_n(Y) = p$ for $(y_1, \dots, y_n) = Y$ means that we reject the null hypothesis with probability p . Each statistical test can make a *type I error* when the hypothesis is falsely rejected with probability $\mathbb{E}_{H_0} \Phi_n(Y)$, and a *type II error* when the hypothesis is falsely accepted with probability $1 - \mathbb{E}_{H_1} \Phi_n(Y)$.

²In our analysis we will couple all parameters to the illumination time t . However, for ease of readability we omit the subscripts t , i.e. we write $n = n_t$ and $d = d_t$ throughout.

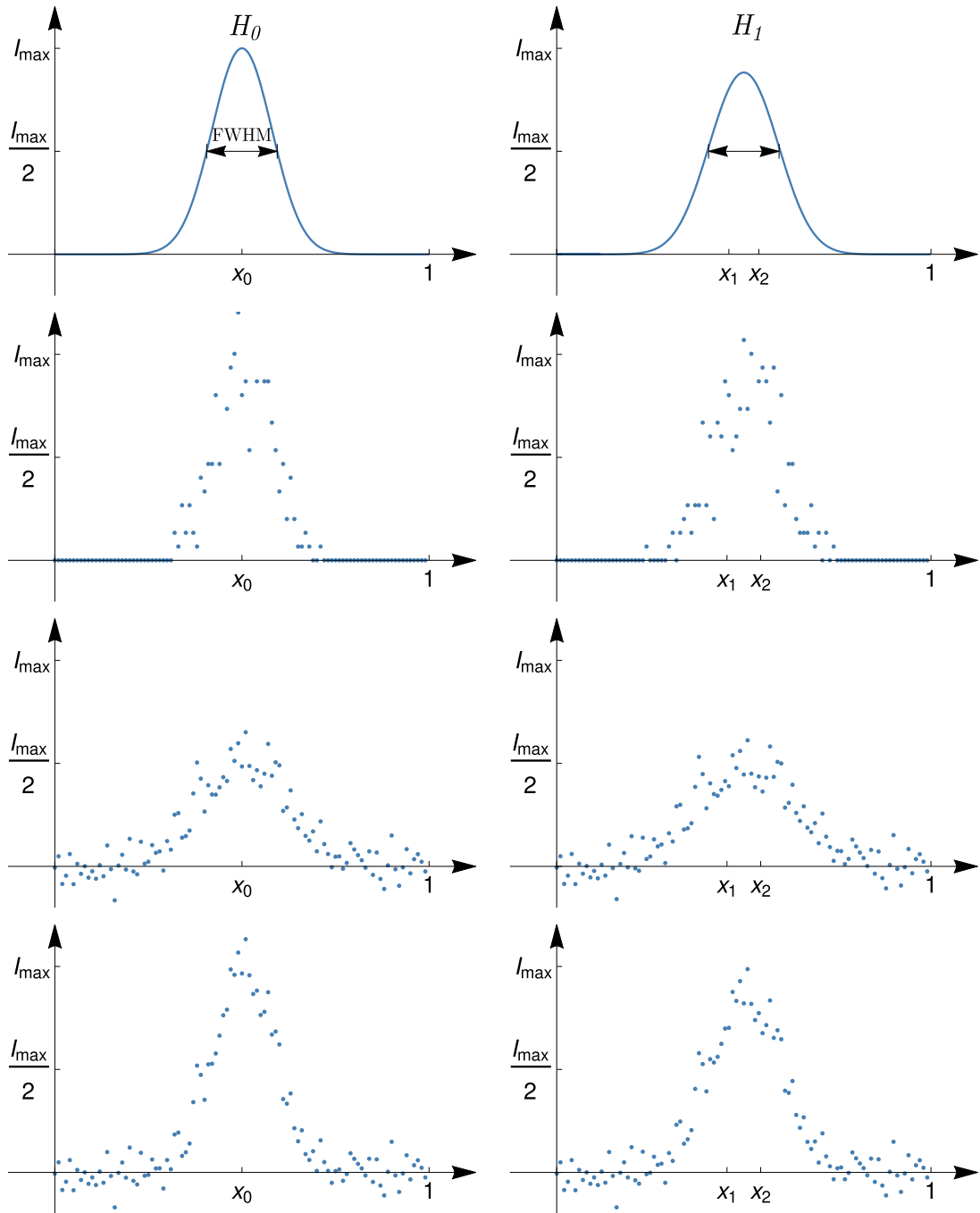


Figure 5: Resolution as a statistical testing problem in one dimension. First row: On the left hand side the hypothesis with the psf centered at x_0 , on the right hand side the alternative with two psfs centered at x_1 and x_2 , distance $d < \text{FWHM}$ apart. Second, third and fourth rows: The corresponding observational data generated according to the Poisson, VSG and HG models, respectively.

As for the locations, the moment x_0, x_1 and x_2 are fixed, H_0 vs. H_1 in (10) constitutes a simple hypothesis vs. a simple alternative testing problem. Thus, according to the Neyman-Pearson lemma [40] for a fixed n and a fixed significance level α , the *likelihood ratio test* (LRT) for H_0 vs. H_1 is uniformly most powerful, i.e. no other statistical test can perform better. For our model (9), the LRT $\Phi_n: \mathbb{R}^n \rightarrow [0, 1]$ takes the form

$$\Phi_n(Y) = \begin{cases} 1 & \text{if } T_n(Y) > q_{\alpha,n}^*, \\ \gamma & \text{if } T_n(Y) = q_{\alpha,n}^*, \\ 0 & \text{if } T_n(Y) < q_{\alpha,n}^*, \end{cases} \quad (11)$$

with the log likelihood ratio statistic $T_n(Y)$ given in terms of the probability mass functions or densities $f_{t\theta}$ of $F_{t\theta}$ by

$$T_n(Y) = \log \left(\frac{\prod_{i=1}^n f_{tp_{1i}}}{\prod_{i=1}^n f_{tp_{0i}}} \right) = \sum_{i=1}^n \log \left(\frac{f_{tp_{1i}}}{f_{tp_{0i}}} \right), \quad (12)$$

which then has to be determined according to the models **(P)**–**(HG)** from Section 1.3. Here and in what follows we abbreviate the detection probabilities in the i th bin by

$$p_{0i} := \int_{(i-1)/n}^{i/n} h(x - x_0) dx \quad (13)$$

under the hypothesis H_0 and

$$p_{1i} := \frac{1}{2} \int_{(i-1)/n}^{i/n} h(x - x_1) dx + \frac{1}{2} \int_{(i-1)/n}^{i/n} h(x - x_2) dx \quad (14)$$

under the alternative H_1 .

Given a significance level $\alpha \in (0, 1)$, the threshold $q_{\alpha,n}^*$ and the constant γ in (11) have to be chosen such that $\mathbb{E}_{H_0} \Phi_n(Y) = \mathbb{P}_{H_0}(T_n(Y) > q_{\alpha,n}^*) + \gamma \mathbb{P}_{H_0}(T_n(Y) = q_{\alpha,n}^*) = \alpha$, as this ensures α to be the level (i.e. the probability of the type I error) of the test.

In the following we adopt a minimax testing point of view. To this end, we begin by determining which choice of x_1 and x_2 in (10) is the most difficult to detect.

Theorem 1.3. *Consider the testing problem (10) for $x_0 = 1/2$ fixed. Assume that the psf h is even. Let $0 < \alpha < 1/2$ and consider the asymptotic regime that $t, n \rightarrow \infty$ and $d \rightarrow 0$. Then for each of the three models defined in Section 1.3 the uniformly most powerful test Ψ^* (and hence the LRT) for (10) with asymptotic level α (i.e. $\mathbb{E}_{H_0} \Psi^*(Y) \rightarrow \alpha$) has the asymptotically smallest power $\mathbb{E}_{H_1} \Psi^*(Y)$ when*

$$x_0 = \frac{x_1 + x_2}{2},$$

i.e. when x_1 and x_2 are placed symmetrically around x_0 .

With the above preparations in mind, we now propose the following definition for the resolution of a microscope:

Definition 1.4 (Statistical resolution of a microscope). Let $Y = (Y_i)_{i \in \{1, \dots, n\}}$ be as in (9) and let h be the point spread function of the microscope under investigation. Choose one of the three models Poisson, VSG or HG. Let $0 < \alpha, \beta < 1/2$, $x_0 \in [0, 1]$, $t \in \mathbb{N}$ and $n \in \mathbb{N}$ be fixed. We define the microscope's *statistical resolution at point x_0 , discretization n , exposure time t , type I error α and type II error β under the prescribed model* as the unique value $d \in (0, 1)$ such that the uniformly most powerful test (and hence the LRT (11)) Ψ^* for (10) with x_1 and x_2 chosen such that $d = |x_1 - x_2|$ and $x_0 = \frac{1}{2}(x_1 + x_2)$ has exactly level α and power $1 - \beta$, i.e. satisfies

$$\mathbb{E}_{H_0} \Psi^*(Y) = \alpha \quad \text{and} \quad \mathbb{E}_{H_1} \Psi^*(Y) = 1 - \beta.$$

In other words, if the distance d between the two sources x_1 and x_2 in (10) satisfies $|x_1 - x_2| = d$, the statistical resolution is determined by the best possible test with detection power $1 - \beta$ while the error of incorrectly assigning two sources (when only one is present) is controlled by α . It is immediately clear that a larger value of d will result in larger power, and a smaller value of d will result in smaller power, i.e. the power as a function of d is monotonically increasing and furthermore continuous. Thus, the statistical resolution is well-defined. Moreover, for x_1 and x_2 with $|x_1 - x_2| \leq d$ no level α test is able to distinguish H_0 and H_1 with power $\geq 1 - \beta$. Note that, doing so, the sum of errors is bounded by $\alpha + \beta$, which is why we restrict ourselves to the case $\alpha, \beta \in (0, \frac{1}{2})$. Consequently, if $\alpha = 0$ or $\beta = 0$, the resolution is infinite—no method can achieve finite resolution if one of the errors is zero. In the case $\alpha = \beta = \frac{1}{2}$ the test $\Psi \sim \text{Bin}(1, \frac{1}{2})$, hence the resolution is 0 which corresponds to the information of a coin flip to decide between H_0 and H_1 .

The aim of this paper is to study the *asymptotic* behavior (as $n, t \rightarrow \infty$ and $d \rightarrow 0$) of the statistical resolution $d = |x_2 - x_1|$ in the three models from Section 1.3 and to relate our results to the classical Abbe and Rayleigh criteria. Further, we will show that the (asymptotic) behavior of d serves as a good proxy in finite sample situations whenever n and t are sufficiently large and d is sufficiently small, which might be useful for designing experiments. This is investigated in simulations presented in Section 3.

1.5 Main theorem and its consequences

To derive the precise asymptotic behavior of the statistical resolution d of a given (super-resolution) microscope, we have to pose smoothness assumptions on its psf h depending on the employed model.

In the HG model we require the following.

Assumption 1.5 (HG model). Suppose that the psf h is even and non-constant. Furthermore let $h \geq 0$ and $h(\cdot - x_i) \in C^2[0, 1]$ for all $i \in \{0, 1, 2\}$.

The requirement that $h \geq 0$ is natural in view of h being an intensity. The differentiability condition is rather mild and clearly satisfied for the Airy pattern in (3) and its most common approximation by a Gaussian.

In case of the VSG and the Poisson models, we need a stronger condition:

Assumption 1.6 (VSG and P models). Suppose that the psf h is even and non-constant. Furthermore let $h > 0$ and $h(\cdot - x_i) \in C^4[0, 1]$ for all $i \in \{0, 1, 2\}$.

Note that due to compactness of $[0, 1]$, Assumption 1.6 implies that $h \geq c > 0$.

Remark 1.7. We emphasize that the Airy pattern in (3) does not satisfy $h > 0$. However, in accordance with many models considered in the literature it is pertinent to include so-called background contributions, i.e. photons arising from other sources than the psf. Examples of such modeling include [2] and [67], which in the notation of (9) would correspond to $Y_i \sim F_t \int_{B_i} g(x) dx + \gamma/n$ with a positive constant γ and g given by (10). If we were to incorporate this background noise into the psf h and hence due to (2) into the image g , we would obtain (9) with $\tilde{g} = g + \gamma > 0$. From this point of view, the assumption $h > 0$ corresponds to the natural requirement that photons can be detected everywhere. We also note that a Gaussian psf on $[0, 1]$ (17), which is the most commonly used approximation to the Airy pattern (see e.g. [67] or Figure 1B), clearly satisfies Assumption 1.6.

For two sequences $(a_n)_{n \in \mathbb{N}}$ and $(b_n)_{n \in \mathbb{N}}$ we write $a_n \asymp b_n$, $a_n \ll b_n$, $a_n \gg b_n$ and $a_n \sim b_n$ if $\lim_{n \rightarrow \infty} a_n/b_n = 1$, $\lim_{n \rightarrow \infty} a_n/b_n = 0$, $\lim_{n \rightarrow \infty} b_n/a_n = 0$ and $\lim_{n \rightarrow \infty} a_n/b_n = c$ for some constant $c > 0$, respectively. Note that, due to asymptotic considerations, we may restrict to non-randomized tests in what follows, i.e. to set $\gamma = 0$ in (11). Recall that we consider asymptotics as $d \rightarrow 0$ and $n, t \rightarrow \infty$. We are now ready to state our main result on the asymptotic behavior of d .

Theorem 1.8. Assume model (9) and consider the testing problem (10) with $x_0, x_1, x_2 \in (0, 1)$ such that $x_0 = (x_1 + x_2)/2$. Let $0 < \alpha, \beta < 1/2$ be type I and II errors, respectively. For $0 < \nu < 1$ denote by q_ν the ν quantile of the standard normal distribution $\mathcal{N}(0, 1)$.

(a) Poisson model

Let the distribution in (9) be given by $F_{t\theta} = \text{Poi}(t\theta)$ and the psf h satisfy Assumption 1.6. Then the statistical resolution d of the corresponding microscope is

$$d \asymp 2\sqrt{2} \sqrt{q_{1-\beta} - q_\alpha} \left(\int_0^1 \frac{h''(x - x_0)^2}{h(x - x_0)} dx \right)^{-1/4} t^{-1/4}. \quad (15)$$

(b) Variance stabilized Gaussian model

Let the distribution in (9) be given by $F_{t\theta} = \mathcal{N}(2\sqrt{t\theta}, 1)$ and the psf h satisfy Assumption 1.6. Then the statistical resolution d of the corresponding microscope also satisfies (15).

(c) Homogeneous Gaussian model

Let the distribution in (9) be given by $F_{t\theta} = \mathcal{N}(t\theta, 1)$, $n = o(t^2)$ and the psf h satisfy Assumption 1.5. Then the statistical resolution d of the corresponding microscope is

$$d \asymp 2\sqrt{2} \sqrt{q_{1-\beta} - q_\alpha} \left(\int_0^1 h''(x - x_0)^2 dx \right)^{-1/4} t^{-1/2} n^{1/4}. \quad (16)$$

Remark 1.9. The assumption $n = o(t^2)$ for the HG model is necessary to get $d \searrow 0$ asymptotically as $t, n \rightarrow \infty$. This assumption is not restrictive for modern microscopy—in most modern experiments there is at least one photon per pixel [67] already from the background, i.e. $t \geq n$ seems natural.

1.6 Strategy of the proof

Let us briefly comment on the techniques employed in the proof of Theorem 1.8. In both Gaussian models, the level and power of the LRT can be computed explicitly. The formulas (15) and (16) are then derived by straightforward approximations of integrals by sums as $t, n \rightarrow \infty$ and $d \rightarrow 0$. In the Poisson model, the analysis is more difficult, as the LRT statistic consists of n weighted Poisson random variables of varying intensity which might tend to any value in $[0, \infty]$ depending on the asymptotic relation between t and n . We prove a CLT for the LRT statistic in case of $t \ll n^{2-\delta}$ for some constant $\delta > 0$. If $t \gg \sqrt{n} \log^8 n$, we can exploit recent results from [52] stating that the Poisson model is asymptotically equivalent in the Le Cam sense to the VSG model and hence (15) holds true. Hence, both regimes together cover the whole parameter space. Note that in the overlapping regime there is no contradiction, since in both regimes we get the same asymptotic statistical resolution.

1.7 Physical implications

Since in most microscopy experiments type I and type II errors are of equal importance, for the rest of this section we set the type I and II errors to be equal $\beta = \alpha$. To understand the experimental implications of Theorem 1.8, recall that for many (super-resolution) microscopes the psf can be well approximated by a Gaussian kernel

$$h(x - x_0) = \frac{1}{\sqrt{2\pi\sigma^2}} \exp\left(-\frac{1}{2\sigma^2}(x - x_0)^2\right) \quad (17)$$

centered at x_0 with variance $\sigma^2 > 0$, see Figure 1B for an illustration. In this case,

$$\text{FWHM} = 2\sqrt{2 \log 2} \sigma \approx 2.355 \sigma$$

and setting $x_0 = 1/2$, we get

$$\begin{aligned} \int_0^1 h''(x - x_0)^2 dx &= \frac{6\sqrt{\pi}\sigma^3 \operatorname{erf}\left(\frac{1}{2\sigma}\right) + e^{-\frac{1}{4\sigma^2}}(2\sigma^2 - 1)}{16\pi\sigma^8} = \frac{3}{8}\pi^{-1/2} \operatorname{erf}\left(\frac{1}{2\sigma}\right) \sigma^{-5} + o(\sigma^{-5}) \\ &= \frac{3}{8}\pi^{-1/2}\sigma^{-5} + o(\sigma^{-5}), \\ \int_0^1 \frac{h''(x - x_0)^2}{h(x - x_0)} dx &= \frac{2 \operatorname{erf}\left(\frac{1}{2\sqrt{2}\sigma}\right)}{\sigma^4} - \frac{e^{-\frac{1}{8\sigma^2}}(4\sigma^2 + 1)}{4\sqrt{2\pi}\sigma^7} = 2 \operatorname{erf}\left(\frac{1}{2\sqrt{2}\sigma}\right) \sigma^{-4} + o(\sigma^{-4}) \\ &= 2\sigma^{-4} + o(\sigma^{-4}), \end{aligned}$$

as $\sigma \searrow 0$ with the error function

$$\operatorname{erf}(x) = \frac{1}{\sqrt{\pi}} \int_{-x}^x e^{-t^2} dt = 2\Phi(\sqrt{2}x) - 1.$$

Thus, according to (16) we obtain in the **homogeneous Gaussian model** the following asymptotic behavior for the statistical resolution:

$$d \asymp \frac{8\pi^{1/8}}{6^{1/4}} \sqrt{q_{1-\alpha}} \frac{n^{1/4}}{\sqrt{t}} \sigma^{5/4} = \frac{2^{7/8}\pi^{1/8}}{3^{1/4}(\log 2)^{5/8}} \sqrt{q_{1-\alpha}} \frac{n^{1/4}}{\sqrt{t}} \operatorname{FWHM}^{5/4}. \quad (18)$$

Note that this is *not* in agreement with the previously discussed FWHM resolution criterion (5), which postulates a linear dependency of d on the FWHM, see also [19] or [15]. From this point of view it becomes evident that the homogeneous Gaussian model is statistically too simple to capture the actual difficulty of the practical experiment.

In contrast, in the **variance stabilized Gaussian**, and **Poisson** models we compute

$$d \asymp 2^{7/4} \sqrt{q_{1-\alpha}} t^{-1/4} \sigma = \frac{2^{1/4}}{\sqrt{\log 2}} \sqrt{q_{1-\alpha}} t^{-1/4} \operatorname{FWHM}, \quad (19)$$

which shows in fact a linear dependency of d on the FWHM in good agreement with the criteria discussed in Section 1.1. We summarize these results in Table 1. To interpret the results, let us look at the FWHM values in $[0.1, 0.5]$. This interval is well-justified since in practice, e.g. for STED microscopes, the resolution is around 50 nm [28, 19] and for measuring a single molecule, the field of view would naturally be restricted to a region of around 100 – 500 nm. For such FWHM values the ratio between the resolutions of (18) and (19) lies in the interval $[0.795n^{1/4}t^{-1/4}, 1.19n^{1/4}t^{-1/4}]$ with it being equal if $\operatorname{FWHM} \approx 0.250t/n$. Therefore, if $t = n$, then the difference between the homogeneous Gaussian and other models' resolution is $\approx \pm 20\%$. The difference is larger if the discretization n is greater than the illumination time t and vice versa. Moreover, if $n \geq 2.57t$, then the resolution in the homogeneous Gaussian model is always larger than in the other models and hence too pessimistic for short illumination times. It is always smaller if $n \leq 0.498t$ and thus is too optimistic for long illumination times.

Even though we have argued before that $t \geq n$ is a natural assumption due to the background contributions, the case $n \geq t$ is especially interesting in super-resolution microscopy if the background is neglected. In two-dimensional experiments, it is common to scan with bin-sizes of 10×10 nm, which for a single molecule requires around 10×10 bins. For modern dyes, the number of expected photons from one marker can be around 500 in a standard confocal experiment, but in super-resolutions setups, this number can be considerably smaller due to the smaller region of excitation, e.g. around 50 – 100. Hence, in our one-dimensional explanatory setup, values of around 10 for n and 7 – 10 for t are realistic when considering super-resolution setups without background.

Once the value of t has been fixed, the asymptotic statistical resolution (19) allows to compare our results to the classical resolution limits of Abbe (1) and Rayleigh (4). Recall that the FWHM of the Airy pattern is $0.51\lambda/\text{NA}$, and hence both criteria can be read as $c \cdot \operatorname{FWHM}$ with a constant

Error $\alpha = \beta$	0.01	0.05	0.1
Model			
Homogeneous Gaussian	$3.08 t^{-1/4} \text{FWHM}^{5/4}$	$2.59 t^{-1/4} \text{FWHM}^{5/4}$	$2.29 t^{-1/4} \text{FWHM}^{5/4}$
VSG / Poisson	$2.18 t^{-1/4} \text{FWHM}$	$1.83 t^{-1/4} \text{FWHM}$	$1.62 t^{-1/4} \text{FWHM}$

Table 1: Limiting asymptotic statistical resolution as given by Theorem 1.8 for the Gaussian psf (17). For ease of comparison, here we have set $n = t$ in the homogeneous Gaussian model.

$c > 0$. Consequently, we can compute the corresponding value of α such that the right-hand side in (19) equals $c \cdot \text{FWHM}$. The results are shown in Table 2. We find that e.g. for $t = 10$ the Abbe criterion allows for a type I error of roughly 6.81%, whereas the Rayleigh criterion allows only 1.33%. We expect higher number of photons necessary in actual experiments, since we have completely disregarded the background noise by choosing the psf (17).

Error $\alpha = \beta$	$\mathbb{E}[N] = t$				
	10	20	30	40	50
Abbe criterion	6.81%	1.76%	0.494%	0.144%	0.0432%
Rayleigh criterion	1.33%	0.0857%	0.00614%	$4.61 \cdot 10^{-4}\%$	$3.56 \cdot 10^{-5}\%$

Table 2: The type I and II errors ($\alpha = \beta$) such that Abbe or Rayleigh criterion is fulfilled for the VSG and Poisson models for different values of the expected number of photons t in 1D. Here we have assumed a Gaussian psf (17), so the formula (19) can be simply inverted to calculate α .

We can also use (19) to analyze the actual improvement by STED over a classical confocal microscope in our statistical context. To this end, recall that the FWHM is decreased by a factor determined by the maximal intensity within the depletion spot, cf. (6). However, increasing the maximal intensity within the depletion spot automatically reduces the number of emitted and hence observable photons, which leads to an increased statistical error. Even though in practical examples (6) is still a good approximation of the actual resolution [28], we can make this more precise using (19) and explain the well-known observation that, unlike Abbe or Rayleigh criteria would suggest, the resolution improvement is not proportional to the FWHM decrease. In experiments, the parameter ξ in (6) is typically chosen such that $\text{FWHM}_{\text{conf}} \approx 6 \text{FWHM}_{\text{STED}}$. As the expected number of photons is determined by the total amount of light emitted by the dyes, t_{STED} will be significantly smaller than t_{conf} . To estimate t_{STED} , in 1D we can use the first order approximation

$$t_{\text{STED}} \approx \frac{1}{\text{FWHM improvement}} t_{\text{conf}} = \frac{1}{6} t_{\text{conf}}.$$

The rationale behind it is that when the psf is thinned by a factor equal to the FWHM improvement, the same holds for the total number of photons since it is proportional to the integral over the psf. Using (19) this yields

$$d_{\text{STED}} = \frac{1}{6^{3/4}} d_{\text{conf}} \approx \frac{d_{\text{conf}}}{4},$$

i.e. even though the FWHM is decreased by a factor of 6, the resolution is only decreased by a factor of around 4. This agrees quite well with experimental observations, see e.g. [19].

We emphasize that this argumentation is to some extent contradictory to the common interpretation that the resolution depends linearly on the FWHM. However, on the one hand this common interpretation completely disregards the presence of noise, as the criteria in Section 1.1 clearly do. On the other hand, due to the development of more stable dyes, the number of observable photons

has increased during the last decades along with the development of super-resolution microscopes. Thus, the decrease of the FWHM was accompanied by an increase of the signal-to-noise ratio, such that the rule of thumb “resolution \sim FWHM” can still be considered valid. Our results give a mathematically rigorous and explicit formula involving both effects, and at the same time explain the experimental observations quite well.

Note that the above argumentation can be readily extended to the two- or three-dimensional setting, as then the corresponding improvement can be computed for each spatial dimension separately.

1.8 Related work

Investigation of resolution in a statistical setting is not new. The HG model (and variations) was considered in [25, 44, 57, 56, 58] and the Poisson model (and variations) in [30, 32, 2]. However, with the exception of [2], most of these works lack mathematical rigor, whereas [2] instead of defining resolution statistically suggest a redefinition in terms of the power function (37) and do not work out the dependency on the FWHM, see below for more details.

Already in the 1960s, resolution has been investigated from a decision theoretic point of view in signal processing theory. Early references include Harris [25] for the homogeneous Gaussian model and Helstrom [30, 31] for the Poisson model. In [30, 31] Helstrom considered signals consisting of different wavelengths varying in space, noting that using Reiffen and Sherman’s paper [53] on optimum demodulation for time-varying Poisson processes one could consider a signal varying in both space and time. For ease of understanding, we assumed that our psf intensity does not vary with time and is monochromatic, see (3). Harris [25] only calculated the probability of a correct decision (power) without any consideration of the level. Helstrom [30] assumed a CLT and basically obtained type I error and power expressions in the CLT regime 2.3.2 for our Poisson model in his Equation (15). To see this, we have to set $g_0 = q_{\alpha,t,n,d}^* := q_{1-\alpha} \sqrt{\mathbb{V}_{H_0} T_{t,n,d}} + \mathbb{E}_{H_0} T_{t,n,d}$ (46) as the threshold in Helstrom’s theory (which is not specified there), $M_0(x) = p_{0i}$, $M_1(x) = p_{1i}$, where $M(x)$ is the effective photon count rate density at $x \in [-1/2, 1/2]^2$, and change integrals in his work to sums.

In [32] Helstrom went even further than in [30] and considered (10) in the context of quantum information theory, following the statistical paradigm originally set out by Middleton [43]. Among other things, Helstrom found out that P_e , the average of type I and type II errors, converges to $1/2 \exp(-t)$ with increasing distance d . Here t is interpreted as the average number of photons. As expected, the bound tends to zero in the classical regime as $t \rightarrow \infty$. Reassuringly, the form of his combined error probability P_e becomes the same as ours with increasing t . However, Helstrom’s results cannot be transferred to our case due to the quantum information theoretic setting, and his proofs are not mathematically rigorous. Notably, he found that P_e is very close to its asymptotic minimum $1/2 \exp(-t)$ whenever d approximately equals twice the Rayleigh criterion, which led him to define the resolution as twice the Rayleigh limit. Much of the current research on resolution in quantum information theory revolves around trying to design different measurement techniques [65, 66, 48, 42] which would allow to experimentally come as close as possible to the theoretical limits calculated by Helstrom [32]. Some of these measurement techniques have been already confirmed by proof of principle experiments, see e.g. [63], others even applied to biological imaging [61]. We emphasize that our theory is designed to describe everyday microscopy experiments with rather many photons so that Helstrom’s limit $1/2 \exp(-t)$ can be safely disregarded. Even though the mathematical treatment of quantum optics experiments is beyond the scope of this paper, we think that it is a fruitful research direction also for statisticians (see e.g. [70], where the authors have defined a *quantum likelihood ratio*).

We also mention contributions from the field of modern signal processing and engineering, namely the works by Milanfar and collaborators [44, 57, 58], see also [56] for an overview. These authors also investigate resolution in terms of statistical measurement errors, and they derive a dependency of the resolution on the inverse fourth root of the so-called *measurement* signal-to-noise-ratio. Note that this has some similarity with the dependency on t in (15). However, even though resolution is treated as a statistical testing problem, in all these papers a homogeneous

Gaussian model (which is challenged by our analysis) is assumed and they lack some mathematical rigor as well. The same can be said of Terebizh [62] who suggested a statistical definition of resolution for extended objects.

Closest to our paper is the work [2] by Acuña and Horowitz on telescope resolution. There, the testing problem $H_0: d = 0$ vs. $H_1: d > 0$ in a 2D model on a line is considered. This corresponds to our Poisson model, but with explicit constant background noise. Their main quantity of interest is p_{1i} (14) considered as a function of d . Under assumptions on p_{1i} 's roughly corresponding to our assumptions on the psf h , they analyzed the likelihood ratio test in the regime where $t \rightarrow \infty$, but kept the number of measurements (discretization) n fixed and finite. Clearly, a finite value of n will at some point restrict the resolution to be of the order $1/n$, as no information finer than the bin-size can be obtained. Moreover, the mathematical treatment of this regime is substantially simpler, as the LRT statistic is given by a finite sum of independent weighted Poisson random variables, whose intensity tends to ∞ , and hence one obtains a CLT trivially. Acuña and Horowitz [2] also note that there is a different regime with finite fixed t and $n \rightarrow \infty$, but do not treat this. All of our results except for asymptotic equivalence also hold in this regime: See Remarks 2.1 and 2.2, and note that the relation between t and n necessary for Theorem 2.6 is trivially satisfied for constant t . The authors define resolution as the (asymptotic) power function of the likelihood ratio test rather than as a single number, which in some sense, is close to our Definition 1.4. However, we believe that it is not intuitive for practitioners to define the resolution as a probability, since they are used to thinking of resolution as a distance. The main result of [2] is the calculation of this power function in the regime $t \rightarrow \infty$, $n = \text{const}$, which we can reproduce asymptotically for large n and t from our more general results (up to dimension and the explicit constant background noise) if we keep a sum instead of the integral in (15), see Remark 2.2. Note furthermore that the power expression of [2] is only valid if $d = \text{const} \times t^{-1/4}$ in accordance with our result (15). We stress that our results give an explicit dependency on the FWHM.

Finally we mention, that the term ‘super-resolution’ is used in mathematical and statistical communities also in a different context, see [16, 46, 11, 12, 22]. There super-resolution addresses the ways to localize signals with (un)known amplitudes by observing their (noisy) Fourier samples, i.e. samples in the frequency domain. The domain is always assumed to have some cut-off frequency f_c corresponding to the inverse Abbe limit in our context. In contrast, in this paper we assume that the locations of our signals are always *known*, i.e. we will follow the experimentalists’ terminology.

2 Proof of the main Theorem 1.8

In this section we will prove Theorem 1.8. We will do this separately for the three models defined in Section 1.3. We start with the homogeneous and variance stabilized Gaussian models because the proof for the Poisson model relies on them.

Before we start, let us introduce some notation. For functions $f(\cdot - x_0) \in L^1[0, 1]$ let

$$\int_i f := \int_{(i-1)/n}^{i/n} f(x - x_0) dx \quad \text{and} \quad \int_0^1 f := \int_0^1 f(x - x_0) dx. \quad (20)$$

Mostly, we will use it for the psf h and its derivatives. Note that we can rewrite (13) as $p_{0i} = \int_i h$ and provided that Assumption 1.6 holds, we have

$$\int_i h \geq \min_{x \in [0, 1]} \frac{h(x - x_0)}{n} \geq \frac{c}{n} \quad (21)$$

for some constant $c > 0$.

2.1 Homogeneous Gaussian model

Proof of Theorem 1.8 for the HG model. As $F_{t\theta} = \mathcal{N}(t \cdot \theta, 1)$, the LRT statistic in (12) becomes

$$T_{t,n,d}(Y) = \log \left(\frac{\varphi(Y | H_1)}{\varphi(Y | H_0)} \right) = \frac{1}{2} \sum_{i=1}^n (t^2 p_{0i}^2 - t^2 p_{1i}^2 + 2Y_i t (p_{1i} - p_{0i}))$$

with φ the density of a standard normal variate. The corresponding likelihood ratio test (11) is given by

$$\Phi_{t,n,d}(Y) := \begin{cases} 1 & \text{if } T_{t,n,d}(Y) > q_{\alpha,t,n,d}^*, \\ 0 & \text{otherwise,} \end{cases} \quad (22)$$

where $q_{\alpha,t,n,d}^* = \sqrt{2\mu_{t,n,d}} q_{1-\alpha} - \mu_{t,n,d}$ with $q_{1-\alpha}$ the $1 - \alpha$ quantile of $\mathcal{N}(0, 1)$ and

$$\mu_{t,n,d} = \frac{t^2}{2} \sum_{i=1}^n (p_{1i} - p_{0i})^2. \quad (23)$$

For ease of readability, we suppress writing the dependence on t and d , and restrict to the dependence on n in the following.

It holds that under $H_0 : T_n(Y) \sim \mathcal{N}(-\mu_n, 2\mu_n)$ and under $H_1 : T_n(Y) \sim \mathcal{N}(\mu_n, 2\mu_n)$. We calculate

$$\begin{aligned} \mathbb{P}_{H_0}(\mathbf{reject}) &= \mathbb{P}_{H_0}(T_n(Y) > q_{\alpha,n}^*) \\ &= \mathbb{P}\left(-\mu_n + \sqrt{2\mu_n}W > q_{\alpha,n}^*\right) = 1 - \mathbb{P}\left(W \leq \frac{q_{\alpha,n}^* + \mu_n}{\sqrt{2\mu_n}}\right) = \alpha, \end{aligned} \quad (24)$$

where $W \sim \mathcal{N}(0, 1)$. Thus, the test is indeed a level α test.

We want the type II error to be equal to β . Thus, we require

$$\begin{aligned} \beta &= \mathbb{P}_{H_1}(\mathbf{accept}) = \mathbb{P}_{H_1}(T_n(Y) \leq q_{\alpha,n}^*) \\ &= \mathbb{P}\left(\mu_n + \sqrt{2\mu_n}W \leq q_{\alpha,n}^*\right) = \mathbb{P}\left(W \leq q_{1-\alpha} - \sqrt{2\mu_n}\right), \end{aligned} \quad (25)$$

where again $W \sim \mathcal{N}(0, 1)$. This implies that

$$\mu_n = (q_{1-\alpha} - q_\beta)^2 / 2. \quad (26)$$

By definition of μ_n we have (recall (20))

$$\mu_n = \frac{t^2}{2} \sum_{i=1}^n (p_{1i} - p_{0i})^2 = \frac{t^2}{2} \sum_{i=1}^n \left(\int_i \Delta \right)^2,$$

where

$$\Delta(x - x_0) := \frac{1}{2}h(x - x_1) + \frac{1}{2}h(x - x_2) - h(x - x_0)$$

is the difference between the psfs under H_1 and H_0 . Since $h \in C^2[0, 1]$,

$$h(x - x_j) = \sum_{k=0}^2 \frac{h^{(k)}(x - x_0)}{k!} (x_0 - x_j)^k + o((x_0 - x_j)^2). \quad (27)$$

Hence, for $x_0 = (x_1 + x_2)/2$

$$\begin{aligned}\Delta(x - x_0) &= \frac{1}{2} \sum_{k=0}^2 \frac{h^{(k)}(x - x_0)}{k!} (x_0 - x_1)^k + \frac{1}{2} \sum_{k=0}^2 \frac{h^{(k)}(x - x_0)}{k!} (x_0 - x_2)^k - h(x - x_0) \\ &\quad + o((x_0 - x_1)^2 + (x_0 - x_2)^2) \\ &= \frac{1}{4} h''(x - x_0) ((x_0 - x_1)^2 + (x_0 - x_2)^2) + h'(x - x_0)(x_0 - (x_1 + x_2)/2) \\ &\quad + o((x_0 - x_1)^2 + (x_0 - x_2)^2)\end{aligned}\tag{28}$$

$$= \frac{1}{8} h''(x - x_0) d^2 + o(d^2).\tag{29}$$

Thus, we get

$$\begin{aligned}\mu_n &= \frac{t^2}{2} \sum_{i=1}^n (p_{1i} - p_{0i})^2 = \frac{t^2}{2} \sum_{i=1}^n \left(\int_i \Delta \right)^2 = \frac{t^2}{2} \sum_{i=1}^n \left(\frac{d^2}{8} \int_i h'' + o\left(\frac{d^2}{n}\right) \right)^2 \\ &= \frac{t^2}{2} \sum_{i=1}^n \left(\frac{d^4}{64} \left(\int_i h'' \right)^2 + o\left(\frac{d^4}{n^2}\right) \right) = \frac{t^2}{2} \sum_{i=1}^n \frac{d^4}{64} \left(\int_i h'' \right)^2 + o\left(\frac{t^2 d^4}{n}\right)\end{aligned}\tag{30}$$

$$= \frac{t^2 d^4}{128n} \int_0^1 (h'')^2 + o\left(\frac{t^2 d^4}{n}\right),\tag{31}$$

applying Lemma 3.1 from the Appendix. Rearranging (31) for d and using (26) we get the desired relation (16). Hence, d as given in (16) is the asymptotic statistical resolution. \square

Remark 2.1. In the derivation of (30) only $d \searrow 0$ is required. Thus, for a finite n we get

$$d \asymp 2\sqrt{2} \sqrt{q_{1-\beta} - q_\alpha} \left(\sum_{i=1}^n \left(\int_i h'' \right)^2 \right)^{-1/4} t^{-1/2}.$$

2.2 Variance stabilized Gaussian model

Proof of Theorem 1.8 for the VSG model. Let $F_{2\sqrt{t\theta}} = \mathcal{N}(2\sqrt{t\theta}, 1)$, i.e.

$$Y_i \stackrel{\text{indep.}}{\sim} \mathcal{N} \left(2 \left(t \int_{(i-1)/n}^{i/n} g(x - x_0) dx \right)^{1/2}, 1 \right).$$

Then the log-likelihood function is

$$T_{t,n,d}(Y) = \log \left(\frac{\varphi(Y | H_1)}{\varphi(Y | H_0)} \right) = \sum_{i=1}^n \left[2t(p_{0i} - p_{1i}) + 2Y_i \sqrt{t} (\sqrt{p_{1i}} - \sqrt{p_{0i}}) \right]$$

with $p_{\cdot i}$ defined in Equations (13) and (14). We define the corresponding likelihood ratio test as in (22), but this time we set $q_{\alpha,t,n,d}^* = \sqrt{2\nu_{t,n,d}} q_{1-\alpha} - \nu_{t,n,d}$ with

$$\nu_{t,n,d} = 2t \sum_{i=1}^n (\sqrt{p_{1i}} - \sqrt{p_{0i}})^2.$$

The proof is similar to the proof of the homogeneous Gaussian model in Section 2.1. We again skip the indices t and d in what follows.

We have under $H_0 : T_n(Y) \sim \mathcal{N}(-\nu_n, 2\nu_n)$ and under $H_1 : T_n(Y) \sim \mathcal{N}(\nu_n, 2\nu_n)$. We calculate

$$\begin{aligned} \mathbb{P}_{H_0}(\mathbf{reject}) &= \mathbb{P}_{H_0}(T_n(Y) > q_{\alpha,n}^*) \\ &= \mathbb{P}(-\nu_n + \sqrt{2\nu_n}W > q_{\alpha,n}^*) = 1 - \mathbb{P}\left(W \leq \frac{q_{\alpha,n}^* + \nu_n}{\sqrt{2\nu_n}}\right) = \alpha, \end{aligned} \quad (32)$$

where as previously $W \sim \mathcal{N}(0, 1)$. Thus, the test is indeed a level α test.

We want the type II error to be equal to β . Thus, we require

$$\begin{aligned} \beta = \mathbb{P}_{H_1}(\mathbf{accept}) &= \mathbb{P}_{H_1}(T_n(Y) \leq q_{\alpha,n}^*) \\ &= \mathbb{P}(\nu_n + \sqrt{2\nu_n}W \leq \sqrt{2\nu_n}q_{1-\alpha} - \nu_n) = \mathbb{P}(W \leq q_{1-\alpha} - \sqrt{2\nu_n}). \end{aligned} \quad (33)$$

This implies that

$$\nu_n = (q_{1-\alpha} - q_\beta)^2/2 = (q_{1-\beta} - q_\alpha)^2/2, \quad (34)$$

since $q_{1-\gamma} = -q_\gamma$ for quantiles of $\mathcal{N}(0, 1)$. On the other hand, by definition of ν_n we have

$$\nu_n = 2t \sum_{i=1}^n (\sqrt{p_{1i}} - \sqrt{p_{0i}})^2.$$

Using the Taylor series expansion (27) as $d \rightarrow 0$ we get

$$\begin{aligned} (\sqrt{p_{1i}} - \sqrt{p_{0i}})^2 &= \left(\sqrt{\int_i h + \frac{d^2}{8} \int_i h'' + o\left(\frac{d^2}{n}\right)} - \sqrt{\int_i h} \right)^2 \\ &= \left(\sqrt{\int_i h} \sqrt{1 + \frac{d^2 \int_i h''}{8 \int_i h} + o(d^2)} - \sqrt{\int_i h} \right)^2 = \left(\frac{d^2 \int_i h''}{16 \sqrt{\int_i h}} + o\left(\frac{d^2}{\sqrt{n}}\right) \right)^2 \\ &= \frac{d^4}{256} \frac{(\int_i h'')^2}{\int_i h} + o\left(\frac{d^4}{n}\right), \end{aligned} \quad (35)$$

where the $(\int_i h)^{-1}$ terms are well-defined by (21). Thus,

$$\nu_n = 2t \sum_{i=1}^n \left(\frac{d^4}{256} \frac{(\int_i h'')^2}{\int_i h} + o\left(\frac{d^4}{n}\right) \right) = \frac{td^4}{128} \int_0^1 \frac{(h'')^2}{h} + o(td^4) \quad (36)$$

as $n \rightarrow \infty$ by Lemma 3.1 with $f(x) = h''(x - x_0)$ and $g(x) = h(x - x_0)$. Rearranging the last equation for d together with (34) gives (15), as required. \square

Remark 2.2. Just as in the homogeneous Gaussian model (Remark 2.1), we can keep n finite in the above proof, provided that $d \searrow 0$ and $t \rightarrow \infty$. Thus, for finite n it holds

$$d \asymp 2\sqrt{2} \sqrt{q_{1-\beta} - q_\alpha} \left(\sum_{i=1}^n \frac{(\int_i h'')^2}{\int_i h} \right)^{-1/4} t^{-1/4}.$$

From this equation, by solving for $1 - \beta$, we can get an expression for the asymptotic power function ($t \rightarrow \infty$, $n = \text{const.}$)

$$\text{power}(t, d) \asymp \Phi \left(q_\alpha + \sqrt{\sum_{i=1}^n \frac{(\int_i h'')^2}{\int_i h} \frac{d^2 \sqrt{t}}{8}} \right).$$

This regime coincides with the one investigated in [2], where Acuña and Horowitz looked at a 2D Poisson model on a line with constant background noise for telescopes. Their power function can be written as

$$\text{power}(t, d) \asymp \Phi \left(q_\alpha + \sigma_0 \frac{d^2 \sqrt{t}}{8} \right) \quad (37)$$

where t is now interpreted as the telescope exposure time and σ_0 a constant which in 1D neglecting the constant background noise can be written as

$$\sqrt{\kappa \sum_{i=1}^n \left(\int_i h \right)^{-1} \left(\frac{\partial^2}{\partial \left(\frac{d}{2} \right)^2} \Big|_{d=0} \left(\frac{1}{2} \int_{(i-1)/n}^{i/n} h \left(x - x_0 - \frac{d}{2} \right) + h \left(x - x_0 + \frac{d}{2} \right) dx \right) \right)^2}$$

with constant $\kappa > 0$ describing the total intensity of the star in question. Reassuringly, this expression for σ_0 coincides (up to κ) for large n with our factor $\sqrt{\sum_{i=1}^n \frac{(\int_i h'')^2}{\int_i h}}$ by the mean value theorem, i.e. we are able to reproduce the main result of [2] from our more general ones, see also Section 1.8.

2.3 Poisson model

The proof for the Poisson model is split into two parts. If $t \gg \sqrt{n} \log^8 n$, then the Le Cam asymptotic equivalence between the Poisson and the VSG models holds and thus the proof follows from the VSG model. If $t \ll n^{2-\delta}$ for some $\delta > 0$, then a CLT holds and we can prove Theorem 1.8 (a) directly.

2.3.1 Analysis in the asymptotic equivalence regime

We briefly recall the theory of asymptotic equivalence developed by Le Cam [38], [39]. We mostly follow the presentation of [24]. In our context we consider a *statistical experiment*—a set

$$\mathcal{E} = (X, \mathcal{X}, \{P_\theta : \theta \in \Theta\}),$$

where (X, \mathcal{X}) is a measurable space with the parameter set $\Theta \subset \mathbb{R}$, a possibly unbounded interval, and P_θ is an absolutely continuous probability measure with respect to some dominating σ -finite measure μ . Consider a second, possibly easier to tackle, experiment $\mathcal{G} = (Y, \mathcal{Y}, \{Q_\theta : \theta \in \Theta\})$ over the same parameter space Θ . Let further (D, \mathcal{D}) be a measurable space of possible decisions. Then the set of Markov kernels $\kappa : (X, \mathcal{X}) \rightarrow (D, \mathcal{D})$ is the set of randomized decision procedures for the experiment \mathcal{E} . We denote it by $\Pi(\mathcal{E})$. We let $\mathcal{L}(D, \mathcal{D})$ to be the set of all loss functions $L : \Theta \times D \rightarrow [0, \infty)$ such that $0 \leq L(\theta, z) \leq 1$ for all $\theta \in \Theta$ and $z \in D$. Given a decision procedure $\kappa \in \Pi(\mathcal{E})$, the true value $\theta \in \Theta$ and a loss function $L \in \mathcal{L}(D, \mathcal{D})$, the risk is

$$R(\mathcal{E}, \kappa, L, \theta) = \int_X \int_D L(\theta, z) \kappa(x, dz) P_\theta(dx).$$

We define the deficiency as

$$\delta(\mathcal{E}, \mathcal{G}) := \sup_{L \in \mathcal{L}(D, \mathcal{D})} \sup_{\kappa_1 \in \Pi(\mathcal{E})} \inf_{\kappa_2 \in \Pi(\mathcal{G})} \sup_{\theta \in \Theta} |R(\mathcal{E}, \kappa_1, L, \theta) - R(\mathcal{G}, \kappa_2, L, \theta)|$$

with the first supremum ranging over all possible decision spaces (D, \mathcal{D}) . Since deficiency is asymmetric, we define the Le Cam (pseudo) distance as

$$\Delta(\mathcal{E}, \mathcal{G}) := \max\{\delta(\mathcal{E}, \mathcal{G}), \delta(\mathcal{G}, \mathcal{E})\}.$$

Definition 2.3. Two sequences of statistical experiments \mathcal{E}^n and \mathcal{G}^n , $n \in \mathbb{N}$, are *asymptotically equivalent* if

$$\Delta(\mathcal{E}^n, \mathcal{G}^n) \rightarrow 0.$$

We can summarize the implications of the above definition for our analysis in the following proposition.

Proposition 2.4. Let \mathcal{E}_1^n and \mathcal{E}_2^n , $n \in \mathbb{N}$, be two sequences of statistical experiments that are asymptotically equivalent, and let Ψ_1^n and Ψ_2^n be the corresponding optimal tests. Then we have

$$\mathbb{E}_{H_0} \Psi_1^n \rightarrow \alpha \quad \text{and} \quad \mathbb{E}_{H_1} \Psi_1^n \rightarrow 1 - \beta \quad \iff \quad \mathbb{E}_{H_0} \Psi_2^n \rightarrow \alpha \quad \text{and} \quad \mathbb{E}_{H_1} \Psi_2^n \rightarrow 1 - \beta,$$

i.e. the type I error of Ψ_1^n converges to α and the type II error to β if and only if the type I error of Ψ_2^n converges to α and type II error to β . Thus, an asymptotic resolution sequence in the sense of Definition 1.4 for the first sequence of experiments will also be an asymptotic resolution for the second sequence.

The above proposition allows us to transfer the VSG result to the Poisson model in the asymptotic equivalence regime:

Corollary 2.5. Let $0 < \alpha, \beta < 1/2$ be type I and II errors, respectively. Assume that $\sqrt{n} \log^8 n = o(t)$ and Assumption 1.6 are valid. Then Theorem 1.8 (a) holds.

Proof. Our VSG model can be viewed as a Gaussian model

$$Y_i \stackrel{\text{indep.}}{\sim} \mathcal{N}\left(2\sqrt{f_n(i/n)}, 1\right)$$

with

$$f_n(x) = t \int_{x-1/n}^x g(y) \, dy \tag{38}$$

for $x \in [1/n, 1]$. According to Example 4.2 of [24], a sequence of n Poisson observations

$$X_i \stackrel{\text{indep.}}{\sim} \text{Poi}(f(i/n))$$

is asymptotically equivalent to the above Gaussian model with some *fixed function* $f : [0, 1] \rightarrow \mathbb{R}$ provided that f is bounded $c_1 \leq f(x) \leq c_2$ by some absolute constants $c_1, c_2 > 0$ and it is Hölder with exponent $\beta > 1/2$. This result was extended in Theorem 4 of [52] to include functions f which are not bounded away from zero: functions $f = f_n$ that may depend on $n \in \mathbb{N}$, satisfy

$$\inf_x f_n(x) \gg n^{-\beta/(\beta+1)} \log^8 n \tag{39}$$

and f_n are Hölder with $1/2 < \beta \leq 1$. Thus, we only need to extend our f_n 's to functions on $[0, 1]$ and prove that they satisfy the assumptions of Theorem 4 of [52] to complete the proof.

As a first step, extend the image function g to a function on $C^2[-1/n, 1]$ such that

$$n^{-1/2} \log^{8+\delta} n \leq t \int_{-1/n}^0 g(y) \, dy \leq t, \tag{40}$$

for some $\delta > 0$. Then we can extend f_n 's in (38) to $f_n : [0, 1] \rightarrow \mathbb{R}$.

We have that $f_n \leq t$ since $\int_0^1 g = 1$ and $g > 0$, and $f_n \in C^3[0, 1]$ since $g \in C^2[-1/n, 1]$. Hence, f_n is Hölder with $\beta = 1$. Due to the psf h being fixed, our testing problem (10) and Assumption 1.6, for all $x \in [1/n, 1]$ it holds that

$$\int_{x-1/n}^x g(y) \, dy \geq \frac{\min_{x \in [0, 1]} g(x)}{n}.$$

Due to the continuity of g and compactness of $[0, 1]$, $\min_{x \in [0, 1]} g(x) \geq c$ for some constant $c > 0$. Thus,

$$\inf_{x \in [0, 1]} f_n = \inf_{x \in [0, 1]} t \int_{x-1/n}^x g(y) \, dy \geq \min \left\{ c \frac{t}{n}, n^{-1/2} \log^{8+\delta} n \right\} \gg n^{-\frac{1}{2}} \log^8(n),$$

by (40), and hence our assumption $\sqrt{n} \log^8 n = o(t)$ implies (39). Therefore, in this case the Poisson model is equivalent to the VSG model for which Theorem 1.8 (a) holds by the above proof. \square

2.3.2 Analysis in the central limit theorem regime

To finish the proof of Theorem 1.8 under the Poisson model, in this section we will prove a CLT in a different parameter regime than in the regime treated previously based on asymptotic equivalence. The regimes of present and previous sections cover the whole parameter domain, thereby completing the proof.

Here we have (recall (9)) $F_{t\theta} = \text{Poi}(t\theta)$, or more explicitly

$$Y_i \stackrel{\text{indep.}}{\sim} \text{Poi}(\lambda_i) \quad \text{with} \quad \lambda_i = t \int_{(i-1)/n}^{i/n} g(x) dx. \quad (41)$$

Note that $\lambda_{1i} = tp_{1i}$ and $\lambda_{0i} = tp_{0i}$. The likelihood ratio statistic for (10) under the model (41) is

$$T_{t,n,d}(Y) = \log \left(\prod_{i=1}^n e^{-(\lambda_{1i} - \lambda_{0i})} \left(\frac{\lambda_{1i}}{\lambda_{0i}} \right)^{Y_i} \right) = \sum_{i=1}^n Y_i \log \left(\frac{\lambda_{1i}}{\lambda_{0i}} \right).$$

Theorem 2.6 (CLT for Poisson LR). *Assume a psf h satisfies Assumption 1.6 and that $n = t^{1/2+\delta}$ for some $\delta > 0$. Then a CLT holds for $T_{t,n,d}(Y)$ under the hypothesis (10a) and the alternative (10b) as $t, n \rightarrow \infty$ and $d \rightarrow 0$, i.e.*

$$\frac{T_{t,n,d} - \mathbb{E}[T_{t,n,d}]}{\sqrt{\mathbb{V}[T_{t,n,d}]}} \xrightarrow{\mathcal{D}} \mathcal{N}(0, 1).$$

Proof of Theorem 2.6. We apply the Lindeberg-Feller CLT for triangular arrays (see [9]). For ease of readability, we again skip indices t and d in what follows.

Let

$$X_{ni} = a_i Y_i,$$

so that

$$T_n(Y) = \sum_{i=1}^n X_{ni},$$

where as before

$$Y_i \stackrel{\text{indep.}}{\sim} \text{Poi}(\lambda_i) \quad \text{and} \quad a_i := \log \left(\frac{\lambda_{1i}}{\lambda_{0i}} \right).$$

Note that $\lambda_{\cdot i}$ and a_i depend on n as well. We also set $\mu_{ni} = \mathbb{E}[X_{ni}]$, $\sigma_{ni}^2 = \mathbb{V}[X_{ni}]$ and $\tau_n^2 = \sum_{i=1}^n \sigma_{ni}^2$. We need to show (see e.g. [9]) that $\sigma_{ni}^2 < \infty$ and that for all $\varepsilon > 0$ we have

$$L_n(\varepsilon) = \frac{1}{\tau_n^2} \sum_{i=1}^n \int (x - \mu_{ni})^2 \mathbf{1}_{\{|x - \mu_{ni}| > \varepsilon \tau_n\}} d\mathbb{P}_{X_{ni}}(x) \rightarrow 0 \quad \text{as } n \rightarrow \infty.$$

We use the Taylor approximation $\log(1 + y_i) = \sum_{k=0}^2 (-1)^k / (k+1) y_i^{k+1} + o(y_i^3)$ together with (29) to get

$$y_i = \frac{\lambda_{1i}}{\lambda_{0i}} - 1 = \frac{\lambda_{1i} - \lambda_{0i}}{\lambda_{0i}} = \frac{\int_i \Delta}{\int_i h} = \frac{1}{8} \frac{\int_i h''}{\int_i h} d^2 + \frac{1}{384} \frac{\int_i h''''}{\int_i h} d^4 + o(d^4). \quad (42)$$

The $(\int_i h)^{-1}$ terms are well-defined by (21).

Under the hypothesis H_0 it holds

$$\begin{aligned}
\mu_{ni} &= \mathbb{E}_{H_0} X_{ni} = a_i \mathbb{E}_{H_0} Y_i = a_i \lambda_{0i} = a_i t \int_i h = \log(1 + y_i) t \int_i h \\
&= \frac{td^2}{8} \int_i h'' + td^4 \left(-\frac{1}{128} \frac{(\int_i h'')^2}{\int_i h} + \frac{1}{384} \int_i h'''' \right) + O\left(\frac{td^6}{n}\right), \\
\nu_n &= \sum_{i=1}^n \mu_{ni} = \mathbb{E}_{H_0} T_n(Y) = t \sum_{i=1}^n a_i \int_i h = \frac{td^2}{8} \int_0^1 h'' + td^4 \left(-\frac{1}{128} \rho_n + \frac{1}{384} \int_0^1 h'''' \right) + O(td^6), \\
\sigma_{ni}^2 &= \mathbb{V}_{H_0} X_{ni} = a_i^2 \mathbb{V}_{H_0} Y_i = a_i^2 \lambda_{0i} = t \log(1 + y_i)^2 \int_i h = \frac{td^4}{64} \frac{(\int_i h'')^2}{\int_i h} + O\left(\frac{td^6}{n}\right), \\
\tau_n^2 &= \sum_{i=1}^n \sigma_{ni}^2 = \mathbb{V}_{H_0} T_n(Y) = t \sum_{i=1}^n a_i^2 \int_i h = t \sum_{i=1}^n \log(1 + y_i)^2 \int_i h = \frac{td^4}{64} \rho_n + O(td^6)
\end{aligned}$$

with

$$\rho_n := \sum_{i=1}^n \frac{\left(\int_{(i-1)/n}^{i/n} h''(x - x_0) dx \right)^2}{\int_{(i-1)/n}^{i/n} h(x - x_0) dx}.$$

Clearly, it holds that $\sigma_{ni}^2 < \infty$. Applying Lemma 3.1 with $f(x) = h''(x - x_0)$ and $g(x) = h(x - x_0)$ we see that

$$\rho_n = \int_0^1 \frac{h''(x - x_0)^2}{h(x - x_0)} dx + o(1) < \infty$$

and hence

$$\tau_n^2 = \frac{td^4}{64} \int_0^1 \frac{h''(x - x_0)^2}{h(x - x_0)} dx + O(td^6).$$

We consider

$$\begin{aligned}
L_n(\varepsilon) &= \frac{1}{\tau_n^2} \sum_{i=1}^n \sum_{\substack{k \in a_i \mathbb{N}_0 \\ |k - \mu_{ni}| > \varepsilon \tau_n}} (k - \mu_{ni})^2 \mathbb{P}_{H_0}(X_{ni} = k) \\
&= \frac{1}{\tau_n^2} \sum_{i=1}^n \sum_{\substack{l \in \mathbb{N}_0 \\ |a_i l - \mu_{ni}| > \varepsilon \tau_n}} (a_i l - \mu_{ni})^2 \mathbb{P}_{H_0}(Y_i = l).
\end{aligned} \tag{43}$$

Note that if $a_i = 0$, then $|a_i l - \mu_{ni}| = 0$. If $a_i \neq 0$, then the condition $|a_i l - \mu_{ni}| > \varepsilon \tau_n$ on l is equivalent to $l \in \mathcal{D}_{\varepsilon, i}$, where $\mathcal{D}_{\varepsilon, i}$ is the set consisting of all $l \in \mathbb{N}_0$ satisfying

$$\begin{cases} l > \varepsilon \sqrt{t} \frac{\sqrt{\sum_{i=1}^n a_i^2 \int_i h}}{|a_i|} + t \int_i h \\ l < -\varepsilon \sqrt{t} \frac{\sqrt{\sum_{i=1}^n a_i^2 \int_i h}}{|a_i|} + t \int_i h. \end{cases}$$

It holds that

$$\begin{aligned}
a_i &= \log(1 + y_i) = y_i + O(y_i^2) = \frac{\int_i h''}{\int_i h} \frac{d^2}{8} + o(d^2), \\
\sum_{i=1}^n a_i^2 \int_i h &= \sum_{i=1}^n (y_i^2 + O(y_i^3)) \int_i h = \sum_{i=1}^n \frac{(\int_i h'')^2}{\int_i h} \frac{d^4}{64} + o(d^4)
\end{aligned} \tag{44}$$

and thus

$$R_i := \frac{\sqrt{\sum_{i=1}^n a_i^2 \int_i h}}{|a_i|} = O(1).$$

Hence, the domain $\mathcal{D}_{\varepsilon,i}$ is a subset of those indices $l \in \mathbb{N}_0$ such that

$$\begin{cases} \varepsilon\sqrt{t}R + \frac{t}{n}q < l < \infty \\ 0 \leq l < -\varepsilon\sqrt{t}R + \frac{t}{n}\bar{q}, \end{cases} \quad (45)$$

where $R = \min_{i \in \{1, \dots, n\}} R_i$, $q = \min_{x \in [0,1]} h(x - x_0)$ and $\bar{q} = \max_{x \in [0,1]} h(x - x_0) < \infty$, since $h(\cdot - x_0) \in C^4[0,1]$. For $n = t^{1/2+\delta}$ with $\delta > 0$ arbitrary, there are no l 's satisfying the second inequality of (45) for sufficiently large t . Hence, setting $l_0 = \lceil \sqrt{t}(\varepsilon R + t^{-\delta}q) \rceil$ it holds that

$$L_n(\varepsilon) \leq \frac{1}{\tau_n^2} \sum_{i=1}^n \sum_{l=l_0}^{\infty} a_i^2 \left(l - t \int_i h \right)^2 e^{-\lambda_{i0}} \frac{\lambda_{i0}^l}{l!} = \frac{t^2}{\tau_n^2} \sum_{i=1}^n a_i^2 \sum_{l=l_0}^{\infty} \left(\frac{1}{t} - \frac{\int_i h}{l} \right)^2 e^{-\lambda_{i0}} \frac{\lambda_{i0}^l}{(l-1)!}.$$

Moreover,

$$\left(\frac{1}{t} - \frac{\int_i h}{l} \right)^2 \leq \frac{1}{t^2} - 2\frac{q}{tln} + \frac{\bar{q}^2}{l^2n^2} = o(1).$$

Note that (44) also implies that

$$\sum_{i=1}^n a_i^2 = O(nd^4).$$

Thus, we have that

$$L_n(\varepsilon) \leq c' \frac{t^2}{\tau_n^2} \sum_{i=1}^n a_i^2 \sum_{l=l_0}^{\infty} e^{-\lambda_{i0}} \frac{\lambda_{i0}^l}{(l-1)!} \leq cnt \sum_{l=l_0}^{\infty} \frac{l}{(l-1)!} \left(\frac{t}{n} \bar{q} \right)^l = ct^{3/2+\delta} \sum_{l=l_0}^{\infty} \frac{l}{(l-1)!} \left(t^{1/2-\delta} \bar{q} \right)^l,$$

for some constants $c, c' > 0$. Consider

$$\begin{aligned} \sum_{l=a}^{\infty} \frac{(t^{1/2-\delta} \bar{q})^l}{l!} &= \frac{(t^{1/2-\delta} \bar{q})^a}{a!} \left(1 + \sum_{l=a+1}^{\infty} \frac{(t^{1/2-\delta} \bar{q})^l}{l!} \frac{a!}{(t^{1/2-\delta} \bar{q})^a} \right) \\ &= \frac{(t^{1/2-\delta} \bar{q})^a}{a!} \left(1 + \frac{t^{1/2-\delta} \bar{q}}{a+1} + \frac{(t^{1/2-\delta} \bar{q})^2}{(a+1)(a+2)} + \dots \right). \end{aligned}$$

Setting $a = \lceil \sqrt{t}(\varepsilon + t^{-\delta}) \rceil$, second and further terms in the brackets are of order $(\varepsilon^{-1}t^{-\delta})^k$ and so we get

$$1 + \sum_{k=1}^{\infty} (\varepsilon^{-1}t^{-\delta})^k = \frac{1}{1 - \varepsilon^{-1}t^{-\delta}} = O(1).$$

Using Stirling's approximation $\log m! = m \log m - m + O(\log m)$ we have that

$$\begin{aligned} \frac{(t^{1/2-\delta})^a}{a!} &= \frac{\exp(a \log(t^{1/2-\delta}))}{\exp(a \log a - a + O(\log a))} = \exp \left(a \left(\log t^{1/2-\delta} - \log a + 1 \right) + O(\log a) \right) \\ &= \exp \left(\sqrt{t}(\varepsilon + t^{-\delta}) \left(-\log(t^\delta \varepsilon + 1) + 1 + o(1) \right) \right) = O \left((t^\delta \varepsilon + 1)^{-\sqrt{t}(\varepsilon + t^{-\delta})} \right). \end{aligned}$$

In our case the terms are of the form

$$t^{1-2\delta} \bar{q}^2 \sum_{k=a}^{\infty} \frac{(t^{1/2-\delta} \bar{q})^k}{k!} \frac{k+2}{k+1},$$

with $a = \lceil \sqrt{t}(\varepsilon R + t^{-\delta}q) \rceil - 2 \sim \lceil \sqrt{t}(\varepsilon + t^{-\delta}) \rceil$ and $(k+2)/(k+1) \leq 2$. Thus, the above considerations apply and all together we get

$$L_n(\varepsilon) \leq O \left(t^{3/2+\delta} (t^\delta \varepsilon + 1)^{-\sqrt{t}(\varepsilon + t^{-\delta})} \right) \rightarrow 0 \quad \text{as } t, n \rightarrow \infty, d \rightarrow 0.$$

Under the hypothesis H_1 we have

$$\begin{aligned}\mu_{ni} &= \mathbb{E}_{H_1} X_{ni} = a_i \lambda_{1i} = a_i(1+y_i)\lambda_{0i} = \frac{td^2}{8} \int_i h'' + td^4 \left(\frac{1}{128} \frac{(\int_i h'')^2}{\int_i h} + \frac{1}{384} \int_i h'''' \right) + O\left(\frac{td^6}{n}\right), \\ \nu_n &= \sum_{i=1}^n \mu_{ni} = \mathbb{E}_{H_1} T_n(Y) = \sum_{i=1}^n a_i(1+y_i)\lambda_{0i} = \frac{td^2}{8} \int_0^1 h'' + td^4 \left(\frac{1}{128} \rho_n + \frac{1}{384} \int_0^1 h'''' \right) + O(td^6), \\ \sigma_{ni}^2 &= \mathbb{V}_{H_1} X_{ni} = a_i^2 \lambda_{1i} = a_i^2(1+y_i)\lambda_{0i} = \frac{td^4}{64} \frac{(\int_i h'')^2}{\int_i h} + O\left(\frac{td^6}{n}\right), \\ \tau_n^2 &= \sum_{i=1}^n a_i^2(1+y_i)\lambda_{0i} = \sum_{i=1}^n \sigma_{ni}^2 = \frac{td^4}{64} \rho_n + O(td^6)\end{aligned}$$

and hence similar considerations prove Lindeberg's condition in this case. \square

Remark 2.7. Due to $\sigma_{ni}^2/\tau_n^2 \rightarrow 0$ Lindeberg's condition is necessary for the CLT to hold.

Now we can analyze the Poisson LRT

$$\Phi_{t,n,d}(Y) := \begin{cases} 1 & \text{if } T_{t,n,d}(Y) > q_{\alpha,t,n,d}^*, \\ 0 & \text{otherwise,} \end{cases}$$

in the CLT regime above. Here

$$q_{\alpha,t,n,d}^* := q_{1-\alpha} \sqrt{\mathbb{V}_{H_0} T_{t,n,d}} + \mathbb{E}_{H_0} T_{t,n,d}. \quad (46)$$

Proof of Theorem 1.8 (Poisson model in the CLT regime). Again we skip the indices of t and d .

We want to find such $q_{\alpha,n}^*$ that

$$\mathbb{P}_{H_0}(\mathbf{reject}) = \mathbb{P}_{H_0}(T_n(Y) > q_{\alpha,n}^*) = \alpha \quad (47)$$

and

$$\mathbb{P}_{H_1}(\mathbf{accept}) = \mathbb{P}_{H_1}(T_n(Y) \leq q_{\alpha,n}^*) = \beta \quad (48)$$

hold. By the CLT 2.6, Equation (47) holds asymptotically, i.e. for sufficiently large t, n and sufficiently small d , (47) holds exactly with some $\tilde{q}_{\alpha,n}^* = q_{\alpha,n}^* + o(1)$. Similarly, by the CLT 2.6 under H_1 we get Equation (48) with $q_{\alpha,n}^* := \sqrt{\mathbb{V}_{H_1} T_n} q_\beta + \mathbb{E}_{H_1} T_n$. For the quantile to be well-defined, we need to figure out when

$$\sqrt{\mathbb{V}_{H_1} T_n} q_\beta + \mathbb{E}_{H_1} T_n = \sqrt{\mathbb{V}_{H_0} T_n} q_{1-\alpha} + \mathbb{E}_{H_0} T_n + o(1).$$

Using previous calculations it holds that

$$\mathbb{E}_{H_1} T_n - \mathbb{E}_{H_0} T_n = \sum_{i=1}^n y_i \log(1+y_i) \lambda_{0i} = \sum_{i=1}^n \lambda_{0i} (y_i^2 + O(y_i^3))$$

and

$$\sqrt{\mathbb{V}_{H_0} T_n} = \sqrt{\sum_{i=1}^n \lambda_{0i} (y_i^2 + O(y_i^3))} = \sqrt{\mathbb{V}_{H_1} T_n}. \quad (49)$$

Thus, the quantile is well-defined if

$$q_{1-\alpha} \sqrt{\mathbb{V}_{H_0} T_n} - q_\beta \sqrt{\mathbb{V}_{H_1} T_n} = \mathbb{E}_{H_1} T_n - \mathbb{E}_{H_0} T_n + o(1) \iff \quad (50)$$

$$\begin{aligned} & \sqrt{\sum_{i=1}^n \lambda_{0i} (y_i^2 + O(y_i^3))} = q_{1-\alpha} - q_\beta \iff \\ & \frac{\sqrt{td^2}}{8} \sqrt{\int_0^1 \frac{h''(x-x_0)^2}{h(x-x_0)} dx} + o(d^4) = q_{1-\alpha} - q_\beta = q_{1-\beta} - q_\alpha. \end{aligned}$$

Solving for d , we get the desired resolution relation (15). \square

3 Simulations

To investigate the finite sample validity of our asymptotic theory, we have performed simulations exploring the (asymptotic) resolution's d dependence on the illumination time t , FWHM and discretization n , see (18) and (19).

In all simulations we chose the level $\alpha = 0.1$ and determined when the type II error is in the range $\beta \in [0.95\alpha, 1.05\alpha)$. For simplicity, we only describe the simulation in Figure 6 (a) of d vs. FWHM in detail, others were conducted similarly. Throughout the simulation we set discretization $n = 20$ and $d = \text{FWHM}$ as the starting distance between the peaks in the alternative. Then for 10,000 times we generated n independent random variables following the corresponding model (9) under the alternative and calculated the type II error. We then used the bisection method to advance d until the type II error became between 0.95α and 1.05α . We performed the above procedure for the FWHM range $0.15, 0.16, \dots, 0.25$.

3.1 Simulation results

The slopes obtained by log-log plots support our theory well already for small t and n , see left column of Figure 6 and Table 3. We stress that in the Gaussian models we only have to consider $d \searrow 0$, provided that we change the integrals in Theorem 1.8 to sums (Remarks 2.1 and 2.2). Therefore, it is expected that for given t and d the simulations are in general closer to the theoretical results in Theorem 1.8 for the VSG and HG models. This is confirmed by the simulations, where in general the HG simulated values are much closer to the theoretical ones. As a rule of thumb, if $t \geq 500$ and $n \geq 500$, the asymptotic formulas can be used as good approximations, see the right column of Figure 6. In general, increasing the intensity t seems to make asymptotic formulas closer to the simulations than increasing the discretization n . This is displayed in Figure 7 which looks at the (t, n) plane in more detail: The asymptotic formulas get much closer to the simulations when transitioning from (a) with $(50, 50)$ to (c) with $(100, 50)$, than from (a) to (b) with $(50, 100)$.

Model	$d(\text{FWHM})_{emp}$ $d(\text{FWHM})_{th}$	$d(t)_{emp}$ $d(t)_{th}$	$d(n)_{emp}$ $d(n)_{th}$
HG	$1.23 \text{ FWHM}^{1.26}$	$1.17 t^{-0.665}$	$0.0502 n^{0.368}$
	$1.08 \text{ FWHM}^{5/4}$	$0.647 t^{-1/2}$	$0.0685 n^{1/4}$
Poisson VSG	$0.879 \text{ FWHM}^{0.979}$	$0.519 t^{-0.352}$	$0.177 n^{0.00274}$
	$0.873 \text{ FWHM}^{0.975}$	$0.495 t^{-0.336}$	$0.183 n^{-0.00464}$
	0.765 FWHM	$0.323 t^{-1/4}$	0.153

Table 3: Limiting asymptotic statistical resolution as given by Theorem 1.8 for the Gaussian psf (17) for small values of t and n . The entries in $d(\text{FWHM})$ correspond to Figure 6 (a), in $d(t)$ to Figure 6 (c) and in $d(n)$ to Figure 6 (e).

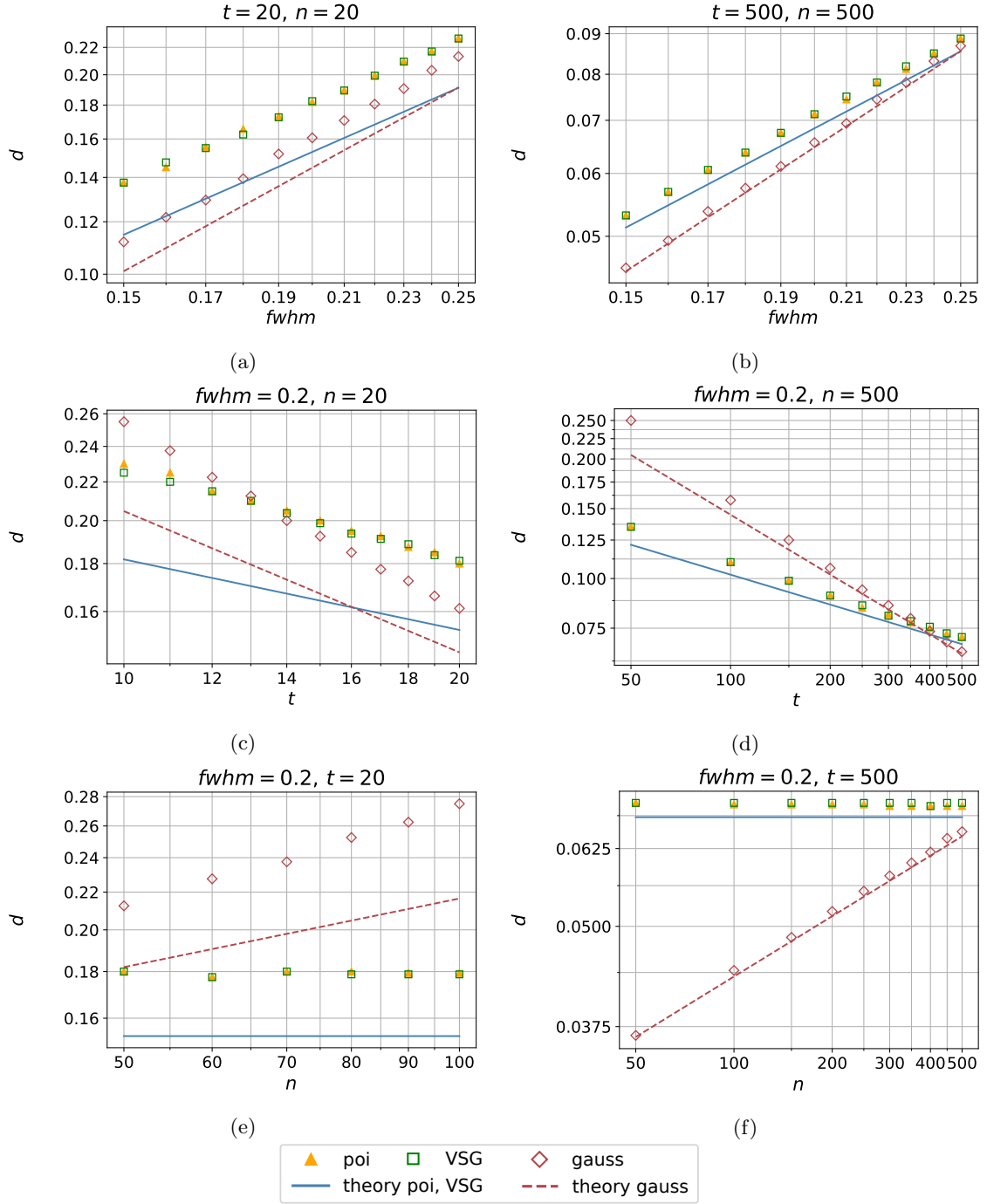


Figure 6: Simulations investigating finite sample validity of the asymptotic relations $d = 2.29 t^{-1/2} n^{1/4} \text{FWHM}^{5/4}$ (18) for the homogeneous Gaussian model, and $d = 1.62 t^{-1/4} \text{FWHM}$ (19) for the VSG and Poisson models, see Section 1.3. Here we have set $\alpha = 0.1$. For short illumination times t and small discretizations n only the slopes of theoretical formulas are close to the slopes obtained from simulations (left column, see also Table 3). As t and n increase, the theoretical formulas become accurate approximations also in terms of absolute error (right column).

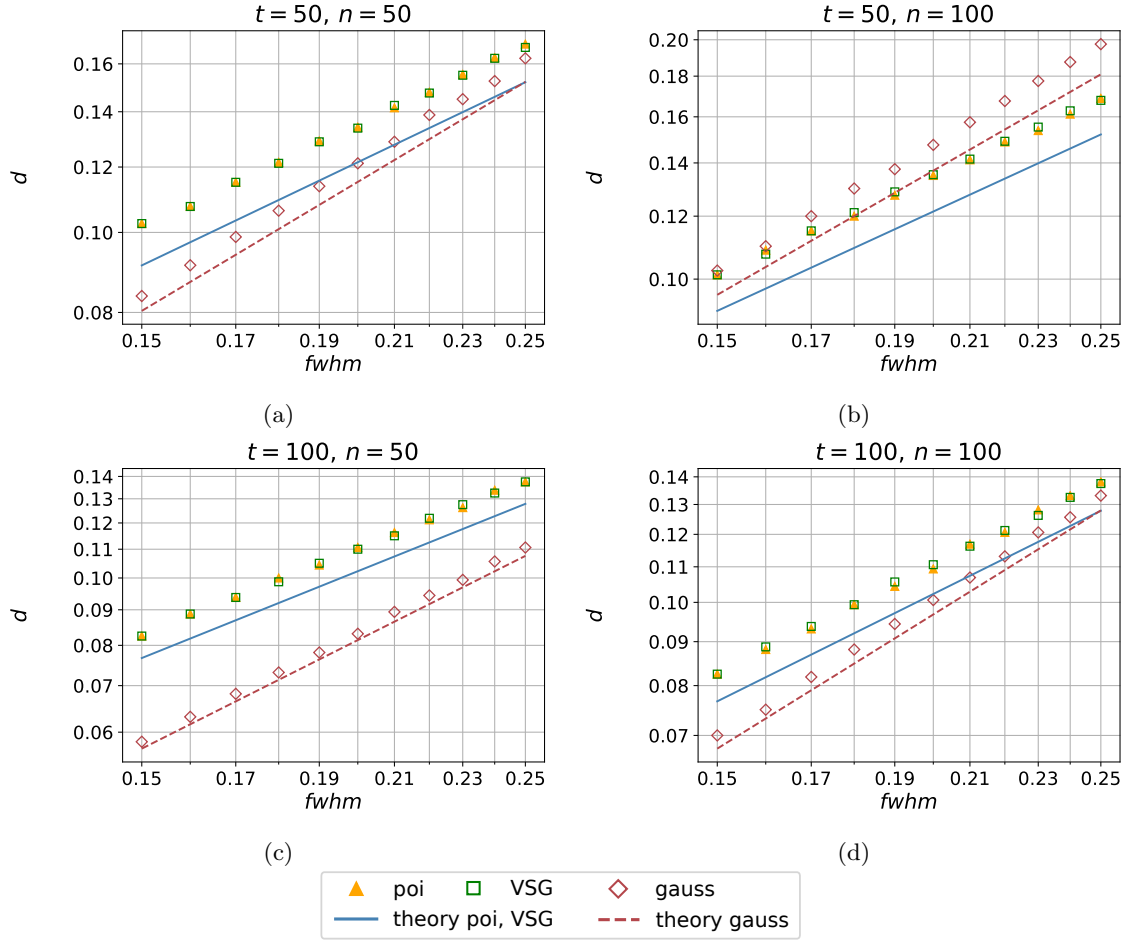


Figure 7: Simulations investigating the finite sample validity of the asymptotic relations $d = 2.29 t^{-1/2} n^{1/4} \text{FWHM}^{5/4}$ (18) for the homogeneous Gaussian model, and $d = 1.62 t^{-1/4} \text{FWHM}$ (19) for the VSG and Poisson models, see Section 1.3. Here we have set $\alpha = 0.1$ and explored the intermediate parameter regime $t = 50, 100$ and $n = 50, 100$.

Appendix: Some auxiliary proofs

3.2 Proof that symmetrically placed signals is the hardest case asymptotically

Proof of Theorem 1.3. We first prove the statement for the **homogeneous Gaussian model**. Let

$$\lambda := \left| x_0 - \frac{x_1 + x_2}{2} \right|.$$

In general, using (28), μ_n as defined in (23) for large n is equal to

$$\begin{aligned} \mu_n = & \frac{t^2}{2n} \left(\frac{\lambda^4}{4} \int_0^1 (h'')^2 + \frac{d^2 \lambda^2}{8} \int_0^1 (h'')^2 + \frac{d^4}{64} \int_0^1 (h'')^2 + \lambda^2 \int_0^1 (h')^2 + \left(\frac{d^2}{4} + \lambda^2 \right) \lambda \int_0^1 h'' h' \right. \\ & \left. + O(\text{higher order terms}) \right). \end{aligned}$$

Since the psf h is even, it holds that $\int_0^1 h'(x-0.5)h''(x-0.5)dx = 0$. Considering μ_n as a function of λ , we find its minimum at $\lambda = 0 + O(d^2)$. Since

$$\text{under } H_0 : T_n(Y) \sim \mathcal{N}(-\mu_n, 2\mu_n),$$

$$\text{under } H_1 : T_n(Y) \sim \mathcal{N}(\mu_n, 2\mu_n),$$

we see that the case $x_0 = \frac{1}{2}(x_1 + x_2)$ is indeed the hardest to distinguish.

The proof for the **variance stabilized Gaussian model** follows the same lines and is therefore omitted.

For the **Poisson** model we have two cases to consider. Whenever $t \gg \sqrt{n} \log^8 n$ we can employ asymptotic equivalence and hence the result follows from the variance stabilized Gaussian model. If $t = n^{2-\delta}$ for some $\delta > 0$, we can prove a CLT also in the asymmetric case. The proof of the CLT is the same as previously (see the proof of Theorem 2.6) just for the ratio

$$R := \min_{j \in \{1, \dots, n\}, |a_j| \neq 0} \frac{\sqrt{\sum_{i=1}^n a_i^2 \int_i h}}{|a_j|}$$

we now use more terms in the series expansion (if $a_j = 0$, then the corresponding summand in (43) is zero). We have

$$y_i = \frac{\lambda_{1i} - \lambda_{0i}}{\lambda_{0i}} = \frac{\int_i \Delta}{\int_i h} = \frac{\int_i h'}{\int_i h} \lambda + \frac{1}{2} \frac{\int_i h''}{\int_i h} \left(\frac{d^2}{4} + \lambda^2 \right) + o(\lambda^2) + o(d^2),$$

$$a_i = \log(1 + y_i) = y_i + O(y_i^2),$$

$$\begin{aligned} \sqrt{\sum_{i=1}^n a_i^2 \int_i h} &= \sqrt{\sum_{i=1}^n \log(1 + y_i)^2 \int_i h} = \sqrt{\sum_{i=1}^n (y_i^2 + O(y_i^3)) \int_i h} \\ &= \sqrt{\sum_{i=1}^n \left(\frac{(\int_i h')^2}{\int_i h} \lambda^2 + \frac{\int_i h' \int_i h''}{\int_i h} \lambda \frac{d^2}{4} + \frac{(\int_i h'')^2}{\int_i h} \frac{d^4}{64} \right) + O(\lambda^3) + o(d^4) + o(\lambda d^2)}, \end{aligned}$$

and thus $R = O(1)$ as before. The rest of the proof is the same as in Theorem 2.6 and is therefore omitted.

The calculation of the asymptotic resolution in the Poisson model essentially boils down to Equation (50) stated here once more for convenience

$$\begin{aligned} q_{1-\alpha} \sqrt{\mathbb{V}_{H_0} T_n} - q_\beta \sqrt{\mathbb{V}_{H_1} T_n} &= \mathbb{E}_{H_1} T_n - \mathbb{E}_{H_0} T_n + o(1) \iff \\ \sqrt{\sum_{i=1}^n \lambda_{0i} (y_i^2 + O(y_i^3))} &= q_{1-\alpha} - q_\beta = q_{1-\beta} - q_\alpha. \end{aligned} \tag{51}$$

Hence, using the above calculations and $\lambda_{0i} = t p_{0i}$, Equation (51) is equivalent to

$$\begin{aligned} t \left(\lambda^2 \int_0^1 \frac{(h')^2}{h} + \frac{d^4}{64} \int_0^1 \frac{(h'')^2}{h} + \lambda \left(\frac{d^2}{4} + \lambda^2 \right) \int_0^1 \frac{h'h''}{h} + o(\lambda^3) + o(d^2 \lambda) + o(d^4) \right) \\ = (q_{1-\beta} - q_\alpha)^2. \end{aligned}$$

Since the psf h is even, h' is odd and h'' is even. Hence,

$$\int_0^1 \frac{h'(x-0.5)h''(x-0.5)}{h(x-0.5)} dx = 0$$

and thus the left hand side considered as a function of λ attains its minimum at $\lambda = 0$. This implies that for given values of α , t and d , the power $1 - \beta$ is the smallest when $\lambda = 0$, i.e. $x_0 = \frac{1}{2}(x_1 + x_2)$, is the most difficult alternative. \square

3.3 An integral approximation

Lemma 3.1. *Let $f : [0, 1] \rightarrow \mathbb{R}$ and $g : [0, 1] \rightarrow \mathbb{R}_{>0}$ be two absolutely continuous functions. Then*

$$\sum_{i=1}^n \frac{\left(\int_{(i-1)/n}^{i/n} f(x) dx \right)^2}{\int_{(i-1)/n}^{i/n} g(x) dx} \xrightarrow{n \rightarrow \infty} \int_0^1 \frac{f(x)^2}{g(x)} dx < \infty.$$

Proof. Note that $f(x)^2/g(x)$ is absolutely continuous, and thus Riemann integrable. Using the mean value theorem we get

$$\begin{aligned} \sum_{i=1}^n \frac{\left(\int_{(i-1)/n}^{i/n} f(x) dx \right)^2}{\int_{(i-1)/n}^{i/n} g(x) dx} &= \frac{1}{n} \sum_{i=1}^n \frac{f(\xi'_i)^2}{g(\xi_i)} + o(1) = \frac{1}{n} \sum_{i=1}^n \frac{(f(\xi'_i) - f(\xi_i) + f(\xi_i))^2}{g(\xi_i)} + o(1) \\ &= \frac{1}{n} \sum_{i=1}^n \frac{(f(\xi'_i) - f(\xi_i))^2 + 2(f(\xi'_i) - f(\xi_i))f(\xi_i) + f(\xi_i)^2}{g(\xi_i)} + o(1) \end{aligned}$$

with $\xi_i, \xi'_i \in [(i-1)/n, i/n]$. Now by continuity of f it holds for all $1 \leq i \leq n$ that

$$|f(\xi_i) - f(\xi'_i)| \leq \max_{x \in [\frac{i-1}{n}, \frac{i}{n}]} f(x) - \min_{x \in [\frac{i-1}{n}, \frac{i}{n}]} f(x) \rightarrow 0,$$

as $n \rightarrow \infty$. Thus, by Riemann integrability

$$\sum_{i=1}^n \frac{\left(\int_{(i-1)/n}^{i/n} f(x) dx \right)^2}{\int_{(i-1)/n}^{i/n} g(x) dx} = \frac{1}{n} \sum_{i=1}^n \frac{f(\xi_i)^2}{g(\xi_i)} + o(1) \rightarrow \int_0^1 \frac{f(x)^2}{g(x)} dx,$$

as $n \rightarrow \infty$. □

3.4 Generalized testing problem with different weights

Consider the generalized testing problem with the hypothesis

$$H_0 : g(x) = h(x - x_0)$$

against the alternative

$$H_1 : g(x) = qh(x - x_1) + (1 - q)h(x - x_2),$$

with $q \in (0, 1)$ and $x_0 = qx_1 + (1 - q)x_2$ fixed. The case considered in the main part of this paper corresponds to $q = 1/2$.

Assume w.l.o.g. that $x_2 \geq x_1$ and let $d = x_2 - x_1$. Note that $x_0 - x_1 = (1 - q)d$ and $x_0 - x_2 = -qd$. Hence, Equation (28) becomes

$$\begin{aligned} \Delta(x - x_0) &:= qh(x - x_1) + (1 - q)h(x - x_2) - h(x - x_0) \\ &= q \sum_{j=0}^2 \frac{h^{(j)}(x - x_0)}{j!} (x_0 - x_1)^j + (1 - q) \sum_{j=0}^2 \frac{h^{(j)}(x - x_0)}{j!} (x_0 - x_2)^j - h(x - x_0) \\ &\quad + o((x_0 - x_1)^2 + (x_0 - x_2)^2) \\ &= \frac{q(1 - q)d^2}{2} h''(x - x_0) + o(d^2). \end{aligned} \tag{53}$$

Homogeneous Gaussian model

Equation (23) becomes

$$\mu_n = \frac{t^2}{2} \sum_{i=1}^n (p_{1i} - p_{0i})^2 = \frac{t^2}{2} \sum_{i=1}^n \left(\int_i \Delta \right)^2 = \frac{t^2 d^4 q^2 (1 - q)^2}{8n} \int_0^1 (h'')^2 + o\left(\frac{t^2 d^4}{n}\right).$$

Just like previously, to have the type I error = α and type II error = β , we have to set $\mu_n = (q_{1-\alpha} - q_\beta)^2/2$, see (24) and (25). Hence, in this case the asymptotic resolution (16) becomes

$$d \asymp \frac{\sqrt{2}}{\sqrt{q(1-q)}} \sqrt{q_{1-\beta} - q_\alpha} \left(\int_0^1 h''(x-x_0)^2 dx \right)^{-1/4} t^{-1/2} n^{1/4}.$$

Thus, the alternative where the psfs have the same weights, i.e. $q = 1/2$, is the *easiest*, since this is the maximum of $q(1-q)$. Also note that as $q \rightarrow 0$ or $q \rightarrow 1$, the resolution $d \rightarrow \infty$, as expected.

Variance stabilized Gaussian model

Using (53) Equation (35) becomes

$$(\sqrt{p_{1i}} - \sqrt{p_{0i}})^2 = \int_i h \left(\sqrt{1 + \frac{\int_i \Delta}{\int_i h}} - 1 \right)^2 = \frac{d^4 q^2 (1-q)^2}{16} \frac{(\int_i h'')}{\int_i h} + o\left(\frac{d^4}{n}\right).$$

Thus, the generalized equivalent of (36) is

$$\nu_n = 2t \sum_{i=1}^n (\sqrt{p_{1i}} - \sqrt{p_{0i}})^2 = \frac{td^4 q^2 (1-q)^2}{8} \int_0^1 \frac{(h'')^2}{h} + o(td^4).$$

As before, by (32) and (33) we have to set $\nu_n = (q_{1-\alpha} - q_\beta)^2/2$ to have the type I error = α and type II error = β . Therefore, in this case the asymptotic resolution is

$$d \asymp \frac{\sqrt{2}}{\sqrt{q(1-q)}} \sqrt{q_{1-\beta} - q_\alpha} \left(\int_0^1 \frac{h''(x-x_0)^2}{h(x-x_0)} dx \right)^{-1/4} t^{-1/4}. \quad (54)$$

Poisson model

First of all, note that the proof in the asymptotic equivalence regime holds by the general VSG model proof above. As for the CLT regime, Equation (42) becomes

$$\begin{aligned} y_i = \frac{\lambda_{1i}}{\lambda_{0i}} - 1 &= \frac{\lambda_{1i} - \lambda_{0i}}{\lambda_{0i}} = \frac{\int_i \Delta}{\int_i h} = \frac{q(1-q)}{2} \frac{\int_i h''}{\int_i h} d^2 + \frac{q(1-q)(1-2q)}{6} \frac{\int_i h'''}{\int_i h} d^3 \\ &+ \frac{q(1-q)((1-q)^2 - q(1-2q))}{24} \frac{\int_i h''''}{\int_i h} d^4 + o(d^4) \end{aligned}$$

and the following terms $\mathbb{E}_{H_0} T_{t,n,d}$, $\mathbb{V}_{H_0} T_{t,n,d}$, $\mathbb{E}_{H_1} T_{t,n,d}$ and $\mathbb{V}_{H_1} T_{t,n,d}$ change accordingly. We skip these expressions due to their length and because they are not particularly insightful. However, it is clear that the CLTs under H_0 and H_1 still hold, just like in the symmetric alternative $q = 1/2$ case.

The crux of the asymptotic resolution determination is Equation (50) which in the general case reads

$$\frac{q(1-q)\sqrt{t}d^2}{2} \sqrt{\int_0^1 \frac{h''(x-x_0)^2}{h(x-x_0)} dx} + o(d^4) = q_{1-\beta} - q_\alpha.$$

Therefore, the asymptotic resolution is the same as in the general VSG model (54).

Remark 3.2. Note that the case $x_0 = qx_1 + (1-q)x_2$ (center of intensity) is the hardest to distinguish in the general testing problem (52) *for even psfs*; the proof easily follows from 3.2 by setting $\lambda = x_0 - (qx_1 + (1-q)x_2)$.

Acknowledgements

We gratefully acknowledge the support of the DFG, CRC 755 ‘‘Nanoscale Photonic Imaging’’, subproject A7, Cluster of Excellence 2067: Multiscale Bioimaging: From molecular medicine to networks of excitable cells (MBExC) and RTG 2088 ‘‘Discovering structure in complex data: Statistics meets Optimization and Inverse Problems’’. We are grateful to Alexander Egner and Jan Keller-Findeisen for helpful comments and discussions.

References

- [1] Abbe, E. (1873). Beiträge zur Theorie des Mikroskops und der mikroskopischen Wahrnehmung. *Archiv für mikroskopische Anatomie*, 9(1):413–418.
- [2] Acuña, C. O. and Horowitz, J. (1997). A statistical approach to the resolution of point sources. *Journal of Applied Statistics*, 24(4):421–436.
- [3] Airy, G. (1835). On the diffraction of an object-glass with circular aperture. *Transactions of the Cambridge Philosophical Society*, 5:283–291.
- [4] Ash, E. A. and Nicholls, G. (1972). Super-resolution aperture scanning microscope. *Nature*, 237:510–512.
- [5] Aspelmeier, T., Egner, A., and Munk, A. (2015). Modern statistical challenges in high-resolution fluorescence microscopy. *Annual Review of Statistics and Its Application*, 2(1):163–202.
- [6] Banterle, N., Bui, K. H., Lemke, E. A., and Beck, M. (2013). Fourier ring correlation as a resolution criterion for super-resolution microscopy. *Journal of Structural Biology*, 183(3):363–367.
- [7] Bertero, M., Boccacci, P., Desider, G., and Vicidomini, G. (2009). Image deblurring with Poisson data: from cells to galaxies. *Inverse Problems*, 25(12):123006.
- [8] Betzig, E., Davidson, M. W., Patterson, G. H., Lippincott-Schwartz, J., Sougrat, R., Lindwasser, O. W., Olenych, S., Bonifacino, J. S., and Hess, H. F. (2006). Imaging intracellular fluorescent proteins at nanometer resolution. *Science*, 313:1642–1645.
- [9] Billingsley, P. (1986). *Probability and Measure*. John Wiley and Sons, 2nd edition.
- [10] Born, M. and Wolf, E. (1999). *Principles of Optics: Electromagnetic Theory of Propagation, Interference and Diffraction of Light*. Cambridge University Press, 7th edition.
- [11] Candès, E. J. and Fernandez-Granda, C. (2013). Super-resolution from noisy data. *Journal of Fourier Analysis and Applications*, 19(6):1229–1254.
- [12] Candès, E. J. and Fernandez-Granda, C. (2014). Towards a mathematical theory of super-resolution. *Communications on Pure and Applied Mathematics*, 67:906–956.
- [13] Courjon, D. (2003). *Near-Field Microscopy and Near-Field Optics*. Imperial College Press, London.
- [14] Cremer, C. and Masters, B. R. (2013). Resolution enhancement techniques in microscopy. *European Physical Journal H*, 38(3):281–344.
- [15] den Dekker, A. J. and van den Bos, A. (1997). Resolution: a survey. *Journal of the Optical Society of America A*, 14(3):547–557.
- [16] Donoho, D. L. (1992). Superresolution via sparsity constraints. *SIAM Journal on Mathematical Analysis*, 23(5):1309–1331.
- [17] Du, C. and Kou, S. C. (2020). Statistical methodology in single-molecule experiments. *Statistical Science*, 35(1):75–91.
- [18] Dürig, U., Pohl, D. W., and Rohner, F. (1986). Near-field optical-scanning microscopy. *Journal of Applied Physics*, 59(10):3318–3327.
- [19] Egner, A., Geisler, C., and Sigmund, R. (2020). Basic knowledge in STED nanoscopy. In Salditt, T., Egner, A., and Luke, R., editors, *Nanoscale Photonic Imaging*. Springer International Publishing.

- [20] Egner, A., Geisler, C., Von Middendorff, C., Bock, H., Wenzel, D., Medda, R., Andresen, M., Stiel, A. C., Jakobs, S., Eggeling, C., Schönle, A., and Hell, S. W. (2007). Fluorescence nanoscopy in whole cells by asynchronous localization of photoswitching emitters. *Biophysical Journal*, 93(9):3285–3290.
- [21] Ehrenberg, M. (2014). Super-resolved fluorescence microscopy. *Scientific Background on Nobel Prize in Chemistry*.
- [22] Fernandez-Granda, C. (2015). Super-resolution of point sources via convex programming. *2015 IEEE 6th International Workshop on Computational Advances in Multi-Sensor Adaptive Processing, CAMSAP 2015*, pages 41–44.
- [23] Goodman, J. W. (1985). *Statistical Optics*. Wiley-Interscience, New York.
- [24] Grama, I. and Nussbaum, M. (2002). Asymptotic equivalence for nonparametric regression. *Mathematical Methods of Statistics*, 11(1):1–36.
- [25] Harris, J. L. (1964). Resolving power and decision theory. *Journal of the Optical Society of America*, 54(5):606–611.
- [26] Heilemann, M., Van De Linde, S., Schüttelpelz, M., Kasper, R., Seefeldt, B., Mukherjee, A., Tinnefeld, P., and Sauer, M. (2008). Subdiffraction-resolution fluorescence imaging with conventional fluorescent probes. *Angewandte Chemie - International Edition*, 47(33):6172–6176.
- [27] Heintzmann, R. and Ficz, G. (2013). Breaking the resolution limit in light microscopy. *Methods in Cell Biology*, 114(4):525–544.
- [28] Hell, S. W. (2007). Far-field optical nanoscopy. *Science*, 316(May):1153–1158.
- [29] Hell, S. W. and Wichmann, J. (1994). Breaking the diffraction resolution limit by stimulated emission: stimulated-emission-depletion fluorescence microscopy. *Optics Letters*, 19(11):780–782.
- [30] Helstrom, C. (1964). The detection and resolution of optical signals. *IEEE Transactions on Information Theory*, 10:275–287.
- [31] Helstrom, C. (1965). Correction to ‘The detection and resolution of optical signals’. *IEEE Transactions on Information Theory*, 11(1):125.
- [32] Helstrom, C. W. (1973). Resolution of point sources of light as analyzed by quantum detection theory. *IEEE Transactions on Information Theory*, 19(4):389–398.
- [33] Hess, S. T., Girirajan, T. P., and Mason, M. D. (2006). Ultra-high resolution imaging by fluorescence photoactivation localization microscopy. *Biophysical Journal*, 91(11):4258–4272.
- [34] Hohage, T. and Werner, F. (2016). Inverse problems with Poisson data: statistical regularization theory, applications and algorithms. *Inverse Problems*, 32(9):093001.
- [35] Houston, W. V. (1927). A compound interferometer for fine structure work. *Physical Review*, 29(3):478–484.
- [36] Huang, B., Bates, M., and Zhuang, X. (2009). Super-resolution fluorescence microscopy. *Annual Review of Biochemistry*, 78(1):993–1016.
- [37] Klar, T. A., Jakobs, S., Dyba, M., Egner, A., and Hell, S. W. (2000). Fluorescence microscopy with diffraction resolution barrier broken by stimulated emission. *Proceedings of the National Academy of Sciences of the United States of America*, 97(15):8206–8210.
- [38] Le Cam, L. (1986). *Asymptotic Methods in Statistical Decision Theory*. Springer Series in Statistics. Springer, New York.

- [39] Le Cam, L. and Yang, G. L. Y. (2000). *Asymptotics in Statistics*. Springer Series in Statistics. Springer, New York.
- [40] Lehmann, E. L. and Romano, J. P. (2005). *Testing Statistical Hypotheses*. Springer Texts in Statistics. Springer, New York, 3rd edition.
- [41] Leonhardt, U. (2010). *Essential Quantum Optics: From Quantum Measurements to Black Holes*. Cambridge University Press.
- [42] Lu, X.-M., Krovi, H., Nair, R., Guha, S., and Shapiro, J. H. (2018). Quantum-optimal detection of one-versus-two incoherent optical sources with arbitrary separation. *npj Quantum Information*, 4(1).
- [43] Middleton, D. (1953). Statistical criteria for the detection of pulsed carriers in noise. I. *Journal of Applied Physics*, 24(4):371–378.
- [44] Milanfar, P. and Shakouri, A. (2002). A statistical analysis of diffraction-limited imaging. In *IEEE International Conference on Image Processing*, pages 864–867.
- [45] Minsky, M. (1961). Microscopy Apparatus. US Patent 3013467, filed 7 November 1957, granted 19 December 1961.
- [46] Morgenshtern, V. I. and Candès, E. J. (2016). Super-resolution of positive sources: the discrete setup. *SIAM Journal on Imaging Sciences*, 9(1):412–444.
- [47] Munk, A., Staudt, T., and Werner, F. (2020). Statistical foundations of nanoscale photonic imaging. In Salditt, T., Egner, A., and Luke, R., editors, *Nanoscale Photonic Imaging*. Springer International Publishing.
- [48] Nair, R. and Tsang, M. (2016). Far-field superresolution of thermal electromagnetic sources at the quantum limit. *Physical Review Letters*, 117(19):190801.
- [49] Orfanidis, S. J. (2016). *Electromagnetic Waves and Antennas*. Rutgers University. Available at <http://eceweb1.rutgers.edu/~orfanidi/ewa/>.
- [50] Oshikane, Y., Kataoka, T., Okuda, M., Hara, S., Inoue, H., and Nakano, M. (2007). Observation of nanostructure by scanning near-field optical microscope with small sphere probe. *Science and Technology of Advanced Materials*, 8(3):181–185.
- [51] Pawley, J. B. (2006). *Handbook of Biological Confocal Microscopy*. Springer, New York, 3rd edition.
- [52] Ray, K. and Schmidt-Hieber, J. (2018). The Le Cam distance between density estimation, Poisson processes and Gaussian white noise. *Mathematical Statistics and Learning*, 1(2):101–170.
- [53] Reiffen, B. and Sherman, H. (1963). An optimum demodulator for Poisson processes: photon source detectors. *IEEE Transactions on Information Theory*, 51(10):1316–1320.
- [54] Rittweger, E., Han, K. Y., Irvine, S. E., Eggeling, C., and Hell, S. W. (2009). STED microscopy reveals crystal colour centres with nanometric resolution. *Nature Photonics*, 3:144–147.
- [55] Rust, M. J., Bates, M., and Zhuang, X. (2006). Sub-diffraction-limit imaging by stochastic optical reconstruction microscopy (STORM). *Nature Methods*, 3(10):793–795.
- [56] Shahram, M. (2005). *Statistical and information-theoretic analysis of resolution in imaging and array processing*. PhD, University of California, Santa Cruz.
- [57] Shahram, M. and Milanfar, P. (2004). Imaging below the diffraction limit: a statistical analysis. *IEEE Transactions on Image Processing*, 13(5):677–689.

- [58] Shahram, M. and Milanfar, P. (2006). Statistical and information-theoretic analysis of resolution in imaging. *IEEE Transactions on Information Theory*, 52(8):3411–3437.
- [59] Staudt, T., Aspelmeier, T., Laitenberger, O., Geisler, C., Egner, A., and Munk, A. (2020). Statistical molecule counting in super-resolution fluorescence microscopy: towards quantitative nanoscopy. *Statistical Science*, 35(1):92–111.
- [60] Strutt, J. W. (1879). XXXI. Investigations in optics, with special reference to the spectroscope. *The London, Edinburgh, and Dublin Philosophical Magazine and Journal of Science*, 8(49):261–274.
- [61] Tenne, R., Rossman, U., Rephael, B., Israel, Y., Krupinski-Ptaszek, A., Lapkiewicz, R., Silberberg, Y., and Oron, D. (2019). Super-resolution enhancement by quantum image scanning microscopy. *Nature Photonics*, 13(2):116–122.
- [62] Terebizh, V. (1995). Image restoration with minimum a priori information. *Uspekhi Fizicheskikh Nauk*, 165(2):143–176.
- [63] Tham, W.-K., Ferretti, H., and Steinberg, A. M. (2017). Beating rayleigh’s curse by imaging using phase information. *Physical Review Letters*, 118:070801.
- [64] Thompson, R. E., Larson, D. R., and Webb, W. W. (2002). Precise nanometer localization analysis for individual fluorescent probes. *Biophysical Journal*, 82(5):2775–2783.
- [65] Tsang, M., Nair, R., and Lu, X.-M. (2016a). Quantum information for semiclassical optics. In *Proceedings of SPIE 10029, Quantum and Nonlinear Optics IV*, page 1002903.
- [66] Tsang, M., Nair, R., and Lu, X. M. (2016b). Quantum theory of superresolution for two incoherent optical point sources. *Physical Review X*, 6(3):031033.
- [67] von Diezmann, A., Shechtman, Y., and Moerner, W. E. (2017). Three-dimensional localization of single molecules for super-resolution imaging and single-particle tracking. *Chemical Reviews*, 117(11):7244–7275.
- [68] Westphal, V. and Hell, S. W. (2005). Nanoscale resolution in the focal plane of an optical microscope. *Physical Review Letters*, 94(April):143903.
- [69] Wouterlood, F. G. (2012). *Cellular Imaging Techniques for Neuroscience and Beyond*. Academic Press.
- [70] Yamagata, K., Fujiwara, A., and Gill, R. D. (2013). Quantum local asymptotic normality based on a new quantum likelihood ratio. *The Annals of Statistics*, 41(4):2197–2217.